nature materials

SUPPLEMENTARY INFORMATION

https://doi.org/10.1038/s41563-019-0305-8

In the format provided by the authors and unedited.

Polymer–inorganic solid–electrolyte interphase for stable lithium metal batteries under lean electrolyte conditions

Yue Gao[1], Zhifei Yan[1], Jennifer L. Gray[2], Xin He[3], Daiwei Wang[4], Tianhang Chen[4], Qingquan Huang[4], Yuguang C. Li[1], Haiying Wang[2], Seong H. Kim[3], Thomas E. Mallouk[1] and Donghai Wang[4]*

[1]Department of Chemistry, The Pennsylvania State University, University Park, PA, USA. [2]Materials Research Institute, The Pennsylvania State University, University Park, PA, USA. [3]Department of Chemical Engineering and Materials Research Institute, The Pennsylvania State University, University Park, PA, USA. [4]Department of Mechanical and Nuclear Engineering, The Pennsylvania State University, University Park, PA, USA. *e-mail: dwang@psu.edu

Table of contents

1. Design and synthesis of the reactive polymeric composite (RPC)

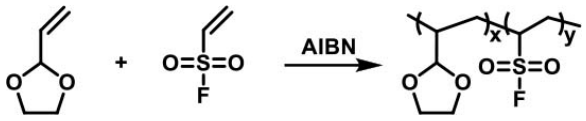

Supplementary Figure 1 | Synthetic route of the poly(vinylsulfonyl fluoride-*ran*-2-vinyl-1,3-dioxolane) polymer. Sulfonyl fluoride and dioxolane building blocks were bulk-polymerized via a free radical polymerization method catalyzed by a 2,2′-azobis(2-methylpropionitrile) (AIBN) initiator.

Supplementary Fig. 1 presents the synthesis of poly(vinyl sulfonyl fluoride-*ran*-2-vinyl-1,3-dioxolane) (P(SF-DOL)) via a free radical copolymerization. Specifically, vinyl sulfonyl fluoride (1.1 g, 10 mmol), 2-vinyl-1,3-dioxolane (2.0 g, 20 mmol), and AIBN (31 mg, 0.19 mmol) were added into a glass vial, and the mixture without any solvent was heated at 67 °C for 48 h. All the procedures were performed in an argon-filled glovebox. The reaction mixture was dissolved in anhydrous dichloromethane (DCM), and the resulting solution was added to anhydrous hexane dropwise. The precipitate was washed with anhydrous hexane 6 times and dried in the vacuum chamber for use. Other functional group-containing polymers were prepared following the same procedure.

To produce organic Li salts as SEI components, we used electrochemically decomposable organic groups, including ethylene oxide (EO), dioxolane (DOL), cyclic ethylene carbonate (CEC), and vinyl carbonate (VC). These groups were connected to the polymer backbone by random copolymerization. After the *on-site* decomposition step, the products preserve the original homogeneity of the polymer. The polymer and GO nanosheets form an integrated composite structure owing to non-covalent interactions between them.

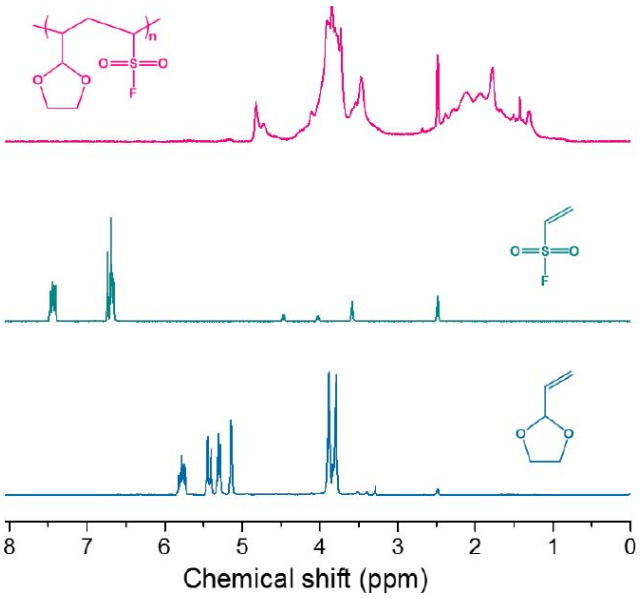

Supplementary Figure 2 | ^{1}H NMR spectra of the P(SF-DOL) polymer.

The structure of P(SF-DOL) was identified by ^{1}H NMR and GPC measurements. The bottom spectrum (blue) of 2-vinyl-1,3-dioxolane shows peaks at 5.85-5.68, 5.36-5.25, and 5.19-5.08 ppm, corresponding to the -CH=CH_2 bond. The middle spectrum (green) of vinylene sulfonyl fluoride presents peaks at 7.50-7.38 and 6.80-6.62 ppm, attributed to the C=C bond. After the reaction (pink), the peaks belonging to C=C bonds disappeared, indicating successful polymerization. The molecular weight (Mw) of P(SF-DOL) based on the GPC calculation was 12,000 g mol^{-1} with a polydispersity index (PDI) of 1.12.

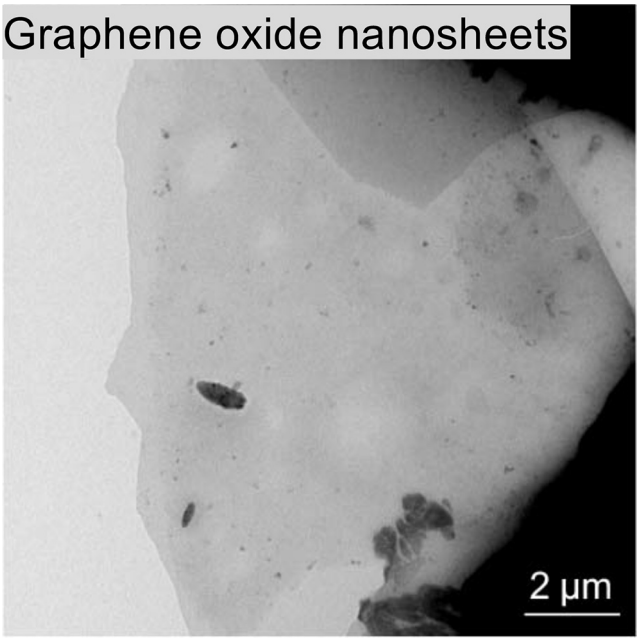

Supplementary Figure 3 | TEM image of as-prepared single-sheet graphene oxide.

Supplementary Fig. 3 shows the morphology of the as-prepared single-sheet GO solution dispersed in anhydrous DMF. The GO nanosheets provide excellent mechanical strength for the RPC-derived SEI.

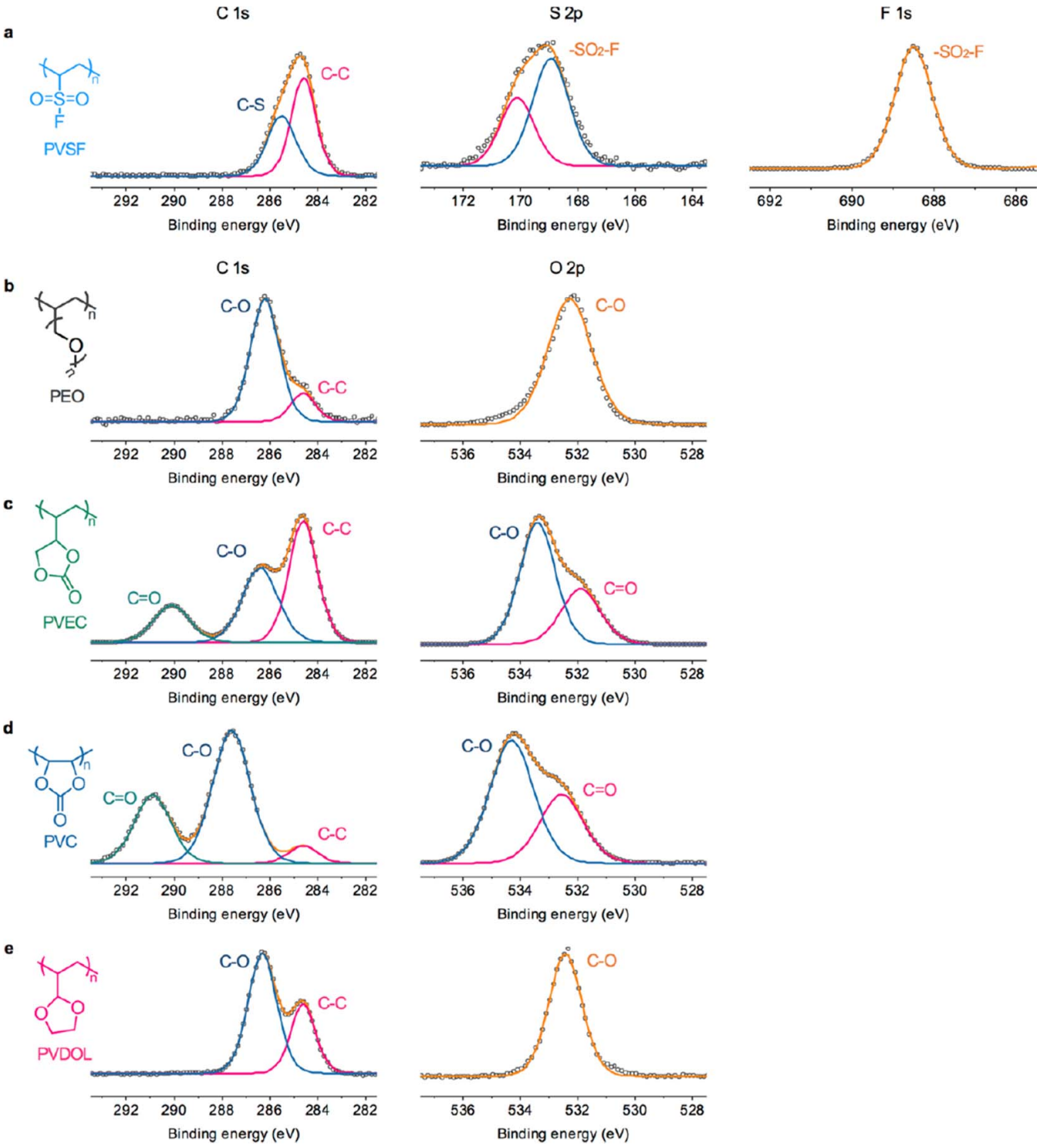

Supplementary Figure 4 | High-resolution XPS spectra of single building block-containing polymers for the RPC design.

The PVSF polymer was synthesized using a vinylene sulfonyl fluoride monomer[1]. In the spectra of the PVSF polymer (Supplementary Fig. 4a), C-S (285.5 eV in the C 1s spectrum), C-C (284.6 eV in the C 1s spectrum), and -SO_2-F (531.9 eV in the O 2p spectrum, 169.4 and 170.6 eV in the S 2p spectrum, and 688.3 eV in the F 1s spectrum) bonds were identified.

The PEO polymer was synthesized using a tetraethylene glycol methyl vinyl ether monomer. In the high-resolution XPS spectra (Supplementary Fig. 4b), C-C (284.6 eV in the C 1s spectrum), C-O (286.2 eV in the C 1s spectrum and 532.3 eV in the O 2p spectrum) bonds were found.

The PVEC polymer was synthesized using a 4-vinyl-1,3-dioxolan-2-one monomer. In the high-resolution XPS spectra (Supplementary Fig. 4c), C-C (284.6 eV in the C 1s spectrum), C-O (286.4 eV in the C 1s spectrum and 533.4 eV in the O 2p spectrum) bonds were detected.

The PVC polymer was synthesized using a vinylene carbonate monomer. In the high-resolution XPS spectra (Supplementary Fig. 4d), C-C (284.6 eV in the C 1s spectrum), C-O (287.6 eV in the C 1s spectrum and 534.3 eV in the O 2p spectrum) were observed. This result is consistent with a previous report[2].

The PVDOL polymer was synthesized using a 2-vinyl-1,3-dioxolane monomer. In the high-resolution XPS spectra (Supplementary Fig. 4e), C-C (284.6 eV in the C 1s spectrum), C-O (286.3 eV in the C 1s spectrum and 532.3 eV in the O 2p spectrum) bonds were observed.

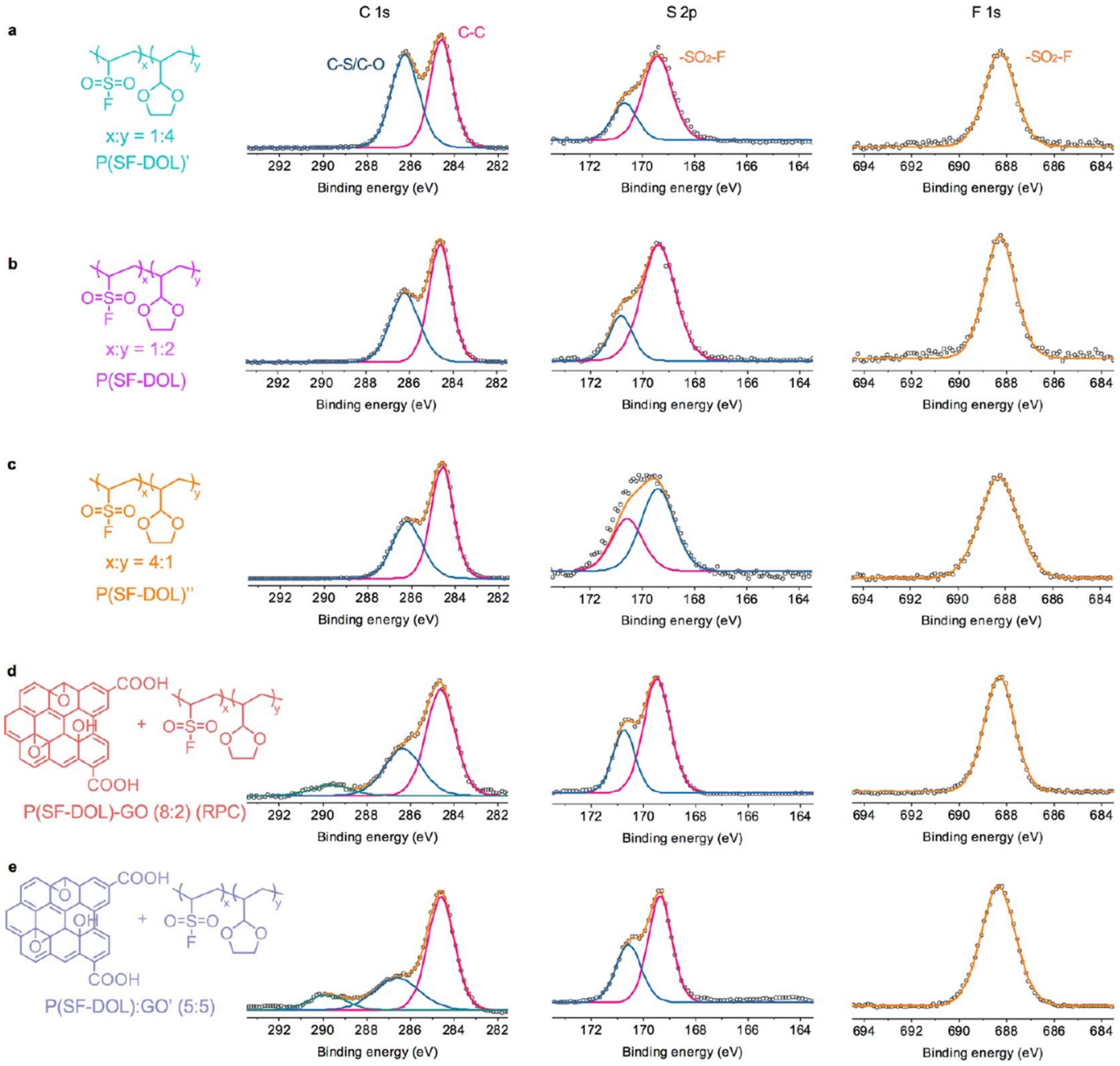

Supplementary Figure 5 | High-resolution XPS spectra of multiple building blocks-containing polymers and polymeric composites for the RPC design.

The P(SF-DOL)' polymer was synthesized using vinylene sulfonyl fluoride and 2-vinyl-1,3-dioxolane monomers with a molar ratio of 1:4. In the spectra of the P(SF-DOL)' polymer (Supplementary Fig. 5a), C-S/C-O (286.3 eV in the C 1s spectrum), C-C (284.6 eV in the C 1s spectrum), and -SO_2-F (688.3 eV in the F 1s spectrum and 169.4 and 170.6 eV in the S 2p spectrum) bonds were identified.

The P(SF-DOL) polymer was synthesized using vinylene sulfonyl fluoride and 2-vinyl-1,3-dioxolane monomers with a molar ratio of 1:2. In the spectra of the P(SF-DOL) polymer (Supplementary Fig. 5b), C-S/C-O (286.3 eV in the C 1s spectrum), C-C (284.6 eV in the C 1s spectrum), and -SO_2-F (688.3 eV in the F 1s spectrum and 169.4 and 170.6 eV in the S 2p spectrum) bonds were identified.

The P(SF-DOL)" polymer was synthesized using vinylene sulfonyl fluoride and 2-vinyl-1,3-dioxolane monomers with a molar ratio of 4:1. In the spectra of the P(SF-DOL)'' polymer (Supplementary Fig. 5c), C-S/C-O (286.3 eV in the C 1s spectrum), C-C (284.6 eV in the C 1s spectrum), and -SO_2-F (688.3 eV in the F 1s spectrum and 169.4 and 170.6 eV in the S 2p spectrum) bonds were identified. 289.6 286.3

The P(SF-DOL)-GO composite was prepared by adding 20% single-sheet GO into the P(SF-DOL) polymer solution. In the high-resolution XPS spectra (Supplementary Fig. 5d), C-C (284.6 eV in the C 1s spectrum), C-O/C-S (286.3 eV in the C 1s spectrum), -CO_2- (289.6 eV in the C 1s spectrum), -SO_2-F (688.3 eV in the F 1s spectrum and 169.4 and 170.6 eV in the S 2p spectrum) groups were observed.

The P(SF-DOL)-GO' composite was prepared by adding 50% single-sheet GO into the P(SF-DOL) polymer solution. In the high-resolution XPS spectra (Supplementary Fig. 5e), C-C (284.6 eV in the C 1s spectrum), C-O/C-S (286.3 eV in the C 1s spectrum), -CO_2- (289.7 eV in the C 1s spectrum), -SO_2-F (688.3 eV in the F 1s spectrum and 169.4 and 170.6 eV in the S 2p spectrum) groups were observed.

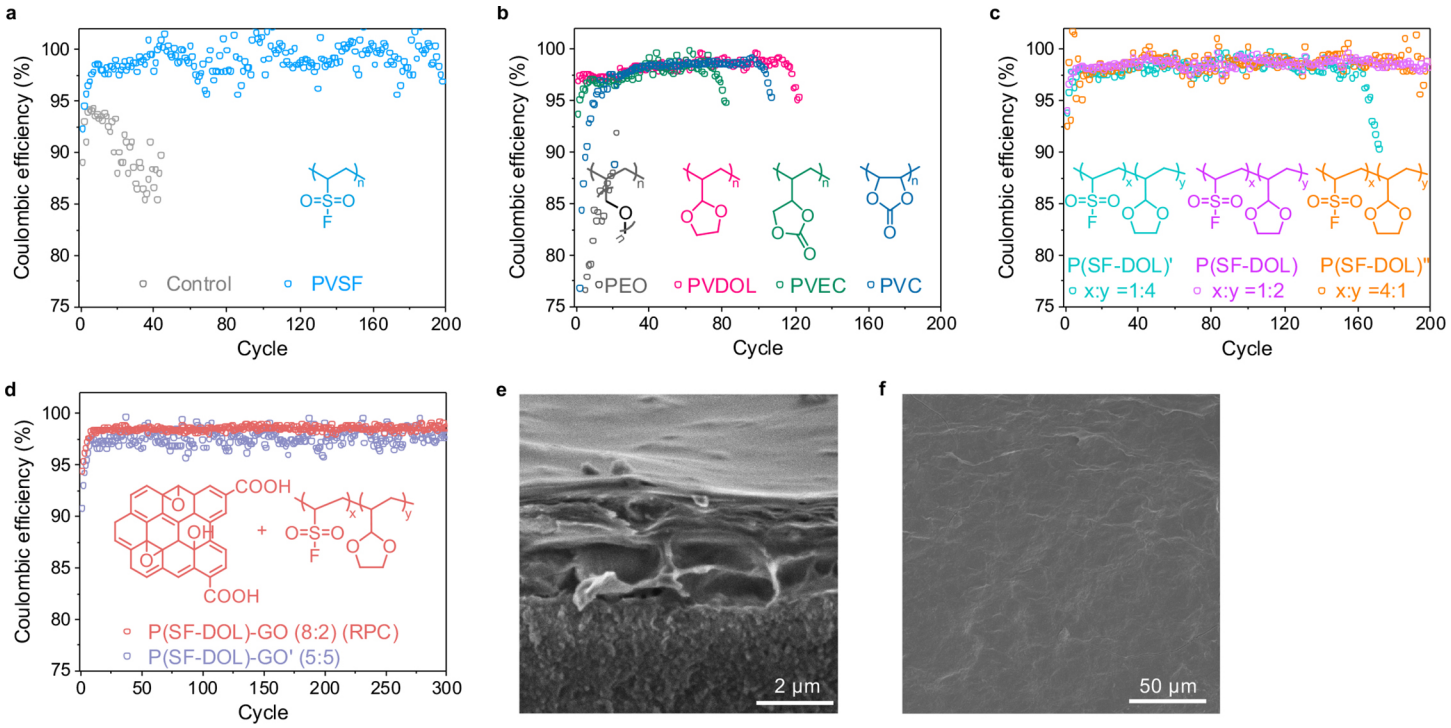

Supplementary Figure 6 | Bottom-up design of the reactive polymeric composite. a-d, Evaluation of various building blocks for constructing the RPC. These building blocks were incorporated into a polymer chain and evaluated via the stability of Li plating and stripping underneath the polymer layer. Sulfonyl fluoride (SF) groups (**a**) were designed to react chemically with Li and generate nanoparticles of LiF. Electrochemically decomposable organic groups (**b**) were designed to generate organic Li salts. The dioxolane (DOL)-containing polymer provides the most enhanced efficiency among these organic building blocks. Combinations of SF and DOL groups in a polymer (**c**) at different molar ratios. The P(SF-DOL) (purple) exhibits both extended cycle life and stable Li deposition. Combinations of P(SF-DOL) and GO nanosheets (**d**) at different weight ratios. The P(SF-DOL)-GO (8:2) composite (red) delivers the optimal Li deposition behavior and less efficiency fluctuation, which was used as the RPC for further studies. The efficiencies were achieved in the Li|Cu cell with a Li deposition capacity of 1.0 mA cm^{-2} at a current density of 0.5 mA cm^{-2}. **e**,**f**, Side- and top-view SEM images of the uncycled RPC-stabilized Li. The RPC layer is uniformly distributed on the Li surface.

We evaluated these building block-containing polymers by studying the stability of Li plating/stripping underneath the polymer film in a Li|Cu cell and the Li deposition morphologies of polymer-coated Li electrodes in a symmetric Li cell. The SF-containing polymer (PVSF) enables 200-cycle (Supplementary Fig. 6a), dendrite-free (Supplementary Fig. 7e) Li deposition. However, the deposition is not stable, indicated by the fluctuating CEs, and some cracks were observed on the polymer-coated surface. Among the polymers tested, the EO-containing polymer (PEO) shows a short cycle life and Li dendrite growth, whereas DOL, EC, and VC-containing polymers (PVDOL, PVEC, and PVC, respectively) lead to stable Li deposition with limited efficiency fluctuation (Supplementary Fig. 6b) and flat surface morphologies with minor defects (Supplementary Fig. 7a-d). PVDOL provided the most extended cycle life. Thus, we combined SF and DOL groups into a random polymer. These polymers gave not only extended cycle lives (Supplementary Fig. 6c) but Li deposition morphologies (Supplementary Fig. 7f-h), compared to that of single building block-containing polymers. The ratio of SF and DOL affects the properties of the polymer. With a 1:2 molar ratio of SF and DOL, the polymer, named P(SF-DOL), shows optimal lifespan and Li deposition morphology. By then adding 20% GO nanosheets into P(SF-DOL), a uniform and integrated composite was formed, due to the strong non-covalent interactions between P(SF-DOL) and GO (Supplementary Fig. 9). This composite displays a layered morphology on the Li surface, captured by SEM images (Supplementary Fig. 6e,f). A 300-cycle (Supplementary Fig. 6d), dendrite-free (Supplementary Fig. 7i) Li deposition behavior was observed. In contrast, the efficiency and morphology of adding excessive GO (50%) in the composites (Supplementary Figs 6d and 7j) and the use of the GO nanosheets alone as an RPC candidate (Supplementary Fig. 8) are not as good as the P(SF-DOL)-GO composite.

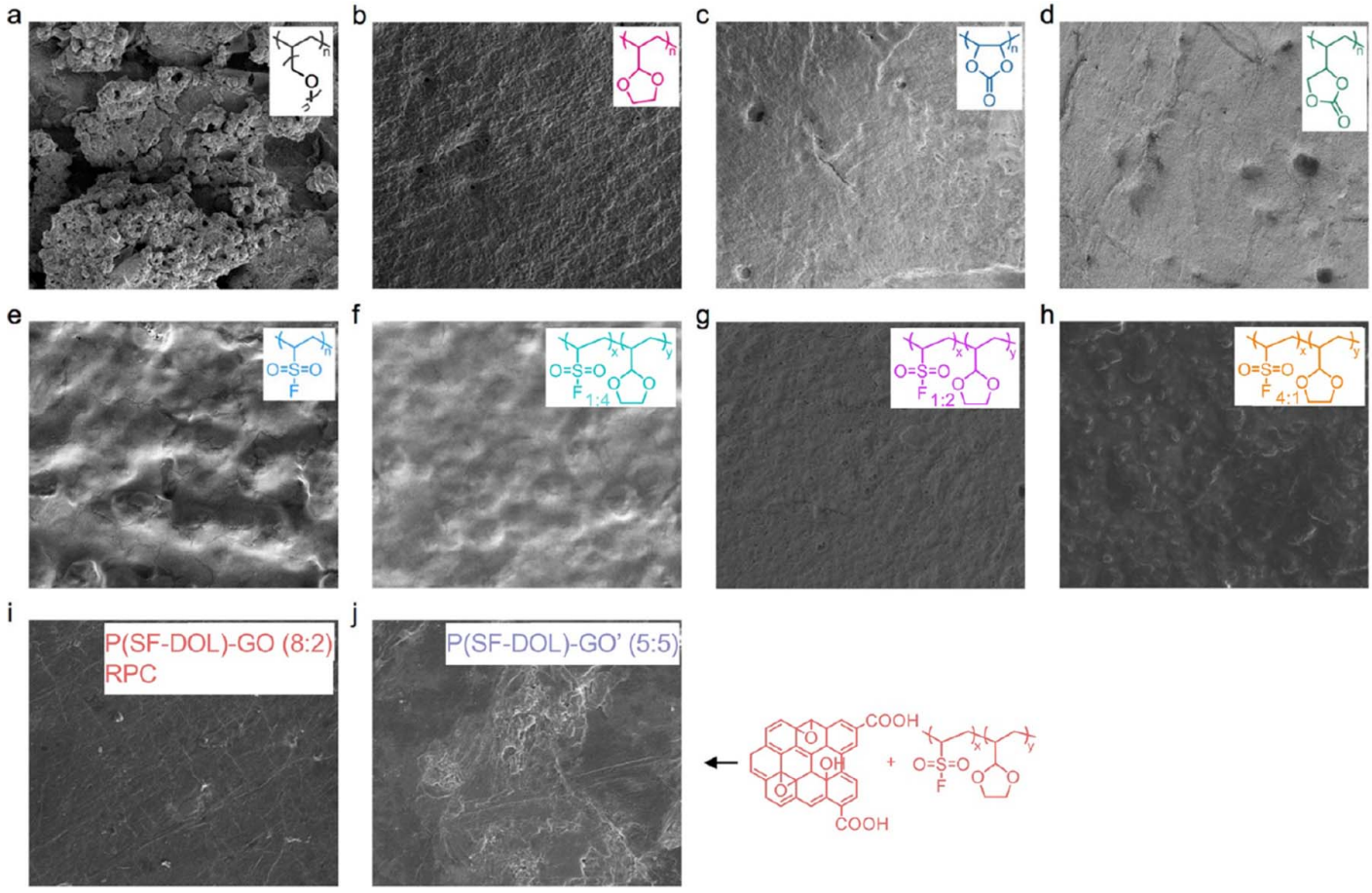

Supplementary Figure 7 | Surface morphologies of the cycled Li with RPC candidates. All Li electrodes were prepared by cycling a Li|Li symmetric cell in a 1 M $LiPF_6$ in EC: EMC: FEC (3:7:1, v/v/v) electrolyte for 10 cycles. The Li plating/stripping amount is 1.0 mAh cm^{-2}.

Based on these testing results, the P(SF-DOL)-GO composite is the optimized RPC and was used for further studies. We emphasize that the efficiencies measured in the Li|Cu cells are not the true efficiency of Li deposition because the SF groups can react with Cu as well. So this measurement is only for the evaluation of the RPC structure. The side reactions between P(SF-DOL) polymer and Cu would hamper its use in "anode-free" systems in which Cu is used as the current collector. To incorporate this approach into the anode-free technology, new current collector materials have to be used, which are chemically stable against sulfonyl fluoride groups. For example, we presented the use of 3D carbon hosts (Fig. 4c and Supplementary Fig. 35a,b) and flat stainless steel foils (Supplementary Fig. 35c) as current collectors to test the efficiency of Li deposition.

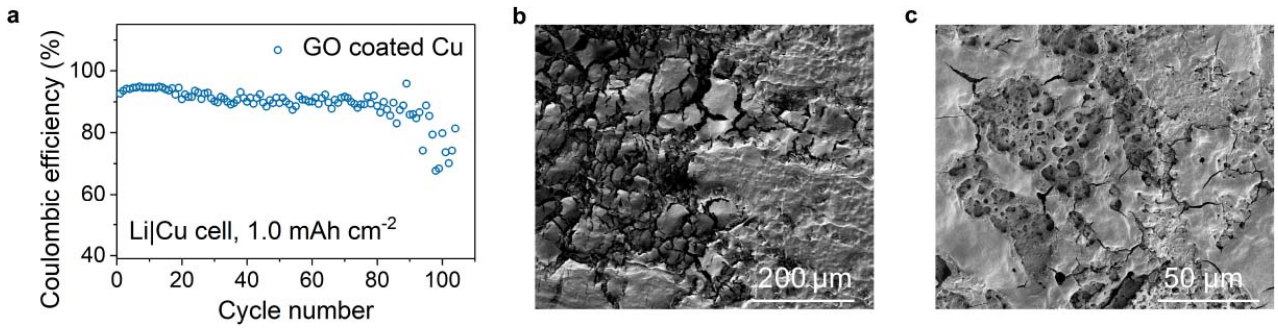

Supplementary Figure 8 | Evaluation of the GO nanosheets layer as an RPC candidate. a, Efficiency of the Li|Cu cell. GO nanosheets was coated on the surface of the Cu electrode. **b**,**c**, Top-view SEM images of the surface morphology of cycled GO-coated Li electrode after 30 cycles in a carbonate electrolyte.

To use GO alone coating layer as an RPC candidate is a good control experiment for investigating the RPC. We have coated a 3 μm GO nanosheets layer on the surface of Li and conducted the Li|Cu cell test and morphology observation. As shown in Supplementary Fig. 8a, the GO coating enabled a 100-cycle life of Li|Cu cell and a low efficiency. The dendrite growth was suppressed, and however, the GO coating layer cannot maintain a good integrity after 30 cycles (Supplementary Fig. 8b,c). These facts are caused by the insufficient functions of the GO coating layer, which can neither form a dense layer and nor regulate the SEI chemistry.

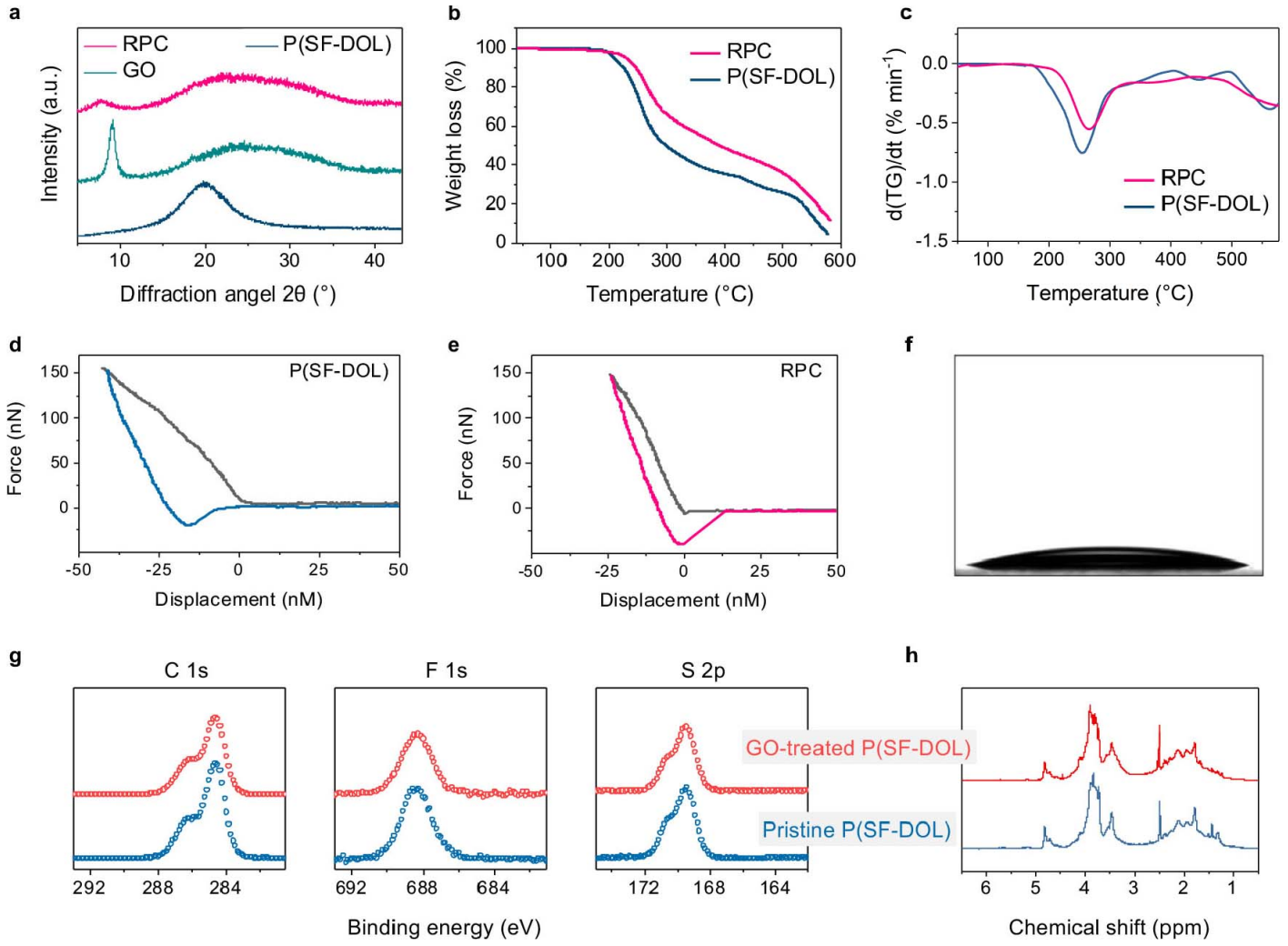

Supplementary Figure 9 | characterization of the integrity of the RPC. a, XRD patterns of the RPC, P(SF-DOL), and GO sheets. **b,c,** TGA curves of the RPC and P(SF-DOL). **d**,**e**, AFM indentation curves of the RPC and P(SF-DOL). **f**, Contact angle between RPC-coated Li and 1 M $LiPF_6$ in EC/EMC electrolyte. **g**, High-resolution C 1s, F 1s, S 2p XPS spectra of the P(SF-DOL) polymer before (blue curves) and after (red curves) being mixed with GO nanosheets in an NMP solution. **h**, ^1H NMR spectra of the P(SF-DOL) polymer before (blue curves) and after (red curves) being mixed with GO nanosheets.

Supplementary Fig. 9a presents the X-ray diffraction (XRD) patterns of the RPC, P(SF-DOL), and GO nanosheets. In the curve of GO nanosheets, the sharp peak at 9.1° is assigned to the GO nanosheet. After forming the composite with P(SF-DOL), the peak shifts to 7.8°, resulting from the non-covalent interactions between the carboxyl and hydroxide groups of the GO and cyclic ether and sulfonyl groups of P(SF-DOL). Supplementary Fig. 9b,c display the thermogravimetric analysis (TGA) curves of the RPC and P(SF-DOL). Compared to P(SF-DOL), the RPC shows increased initial decomposition temperature and the highest decomposition rate temperature. The improved thermostability is also caused by the non-covalent interactions between the P(SF-DOL) and GO nanosheets. Furthermore, the RPC film shows a higher modulus than that of P(SF-DOL), which was measured by AFM indentation (Supplementary Fig. 9d,e). The organic P(SF-DOL) polymer and GO have good affinity to organic electrolyte molecules such as EC, EMC, and FEC, indicated by a contact angle of ~2° between RPC-coated Li and 1 M $LiPF_6$ in EC/EMC electrolyte (Supplementary Fig. 9f).

We have excluded covalent interactions between the polymer and GO because the polymer structure was maintained before and after being mixed with the GO. This was identified by XPS and ^{1}H and ^{19}F NMR analyses. Supplementary Fig. 9g shows high-resolution C 1s, F 1s, and S 2p XPS spectra in which consistent positions of peaks were found, including C-C (284.6 eV in the C 1s spectra), C-S/C-O (286.3 eV in the C 1s spectra), and -SO_2-F (169.4 and 170.6 eV in the S 2p spectra and 688.4 eV in the F 1s spectra). Besides, the ^{1}H NMR (Supplementary Fig. 9h) and ^{19}F NMR (Supplementary Fig. 9i) spectra of the P(SF-DOL) polymer before (blue curves) and after (red curves) being mixed with GO nanosheets are unchanged (Supplementary Fig. 9h,i). The identical XPS and NMR spectra strongly suggest that no covalent bond-forming reaction takes places between the polymer and GO nanosheets.

2. SEI chemistry ruled by the RPC

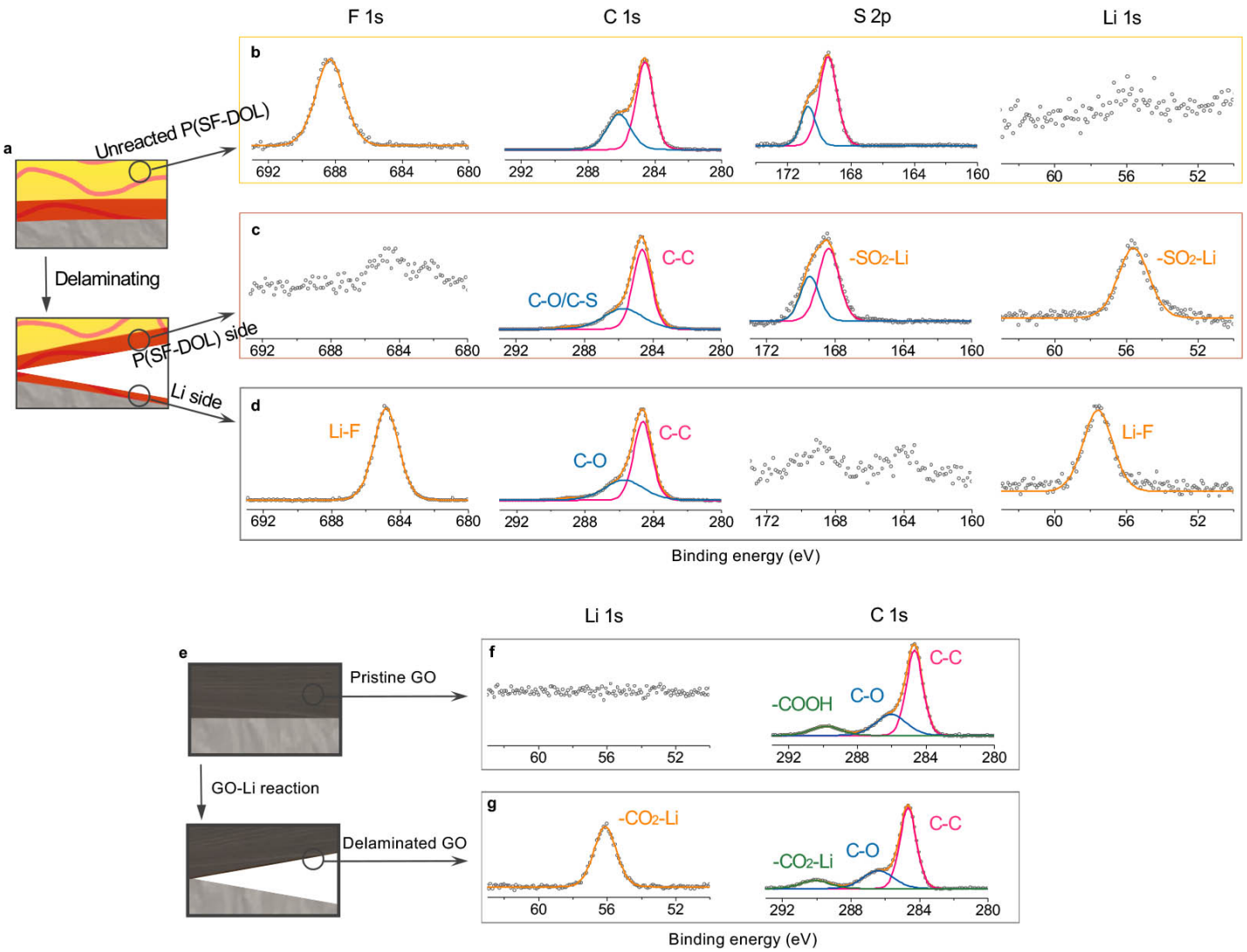

Supplementary Figure 10 | Structure of the surface passivating layer formed in the two-step SEI formation. a, Illustration of the surface passivating layer (red layer) at the interface, which is formed by the chemical reaction between P(SF-DOL) (yellow layer) and Li (grey layer). **b-d**, High-resolution XPS spectra of the unreacted P(SF-DOL) (**b**) and delaminated interface (both the P(SF-DOL) (**c**) and Li (**d**) sides) after the reaction. LiF and a polymer with side groups of -SO_2-Li and -$CHO_2(CH_2)_2$-) were observed at the Li/P(SF-DOL) interface. **e,** Illustration of the reaction between GO nanosheets and Li metal. **f,g**, High-resolution XPS spectra of the pristine GO (**f**) and delaminated interface of GO after the reaction (**g**). -CO_2-Li signals were found at the interface of the delaminated GO film.

We investigated the chemical and electrochemical processes associated with the Li surface passivation and RPC decomposition steps. To study the chemical reaction occurring at the Li surface, we physically pressed a P(SF-DOL) film into a clean Li chip (see Methods for details) and ran high-resolution XPS on the delaminated interface (both the P(SF-DOL) and Li chip sides) after the reaction (Supplementary Fig. 10a). We observed a clear change in the chemical structure at the interface from the structure of the unreacted P(SF-DOL) (Supplementary Fig. 10b). On the P(SF-DOL) side (Supplementary Fig. 10c),), -SO_2-F (169.4 and 170.6 eV in the S 2p spectrum and 688.3 in the F 1s spectrum) was converted into -SO_2-Li (peaks at 168.3 and 169.5 in the S 2p spectrum and 55.6 eV in the Li 1s spectrum)[3]. Compared with the spectra of pristine P(SF-DOL) (Supplementary Fig. 5b), no noticeable change in the C 1s spectrum was found, indicating retention of the polymer backbone. Meanwhile, LiF appeared on the Li side (Supplementary Fig. 10d), as evidenced by peaks at 684.8 in the F 1s spectrum and 57.6 eV in the Li 1s spectrum. The unreacted P(SF-DOL) (Supplementary Fig. 10a) remains intact, as verified by the presence of the same peaks as in the spectra of pristine P(SF-DOL) (Supplementary Fig. 5b).

To investigate the chemical reactions between the GO and Li, we physically attached a GO film onto a freshly cleaned Li chip and ran high-resolution XPS on the delaminated surface of the GO film (Supplementary Fig. 10e). We found -CO_2-Li groups (peaks at 56.1 eV in the Li 1s spectrum and 289.9 eV in the C 1s spectrum) on the surface of the delaminated GO film (Supplementary Fig. 10f), in contrast to the absence of Li signals in the spectra of the pristine GO film (Supplementary Fig. 10g).

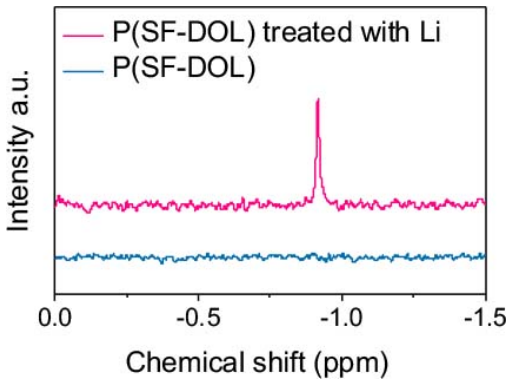

Supplementary Figure 11 | ^{7}Li NMR spectrum of the products of the chemical reaction between P(SF-DOL) and Li.

We also conducted ^{7}Li NMR experiments to monitor the bulk reaction between P(SF-DOL) and Li (see Methods for details). A single peak with a chemical shift of -0.92 ppm was observed in the ^{7}Li NMR spectrum of the reaction solution (Supplementary Fig. 11), which can be assigned to -SO_2-Li[4]. Based on these results, we identified the formation of a surface passivating layer at the Li/RPC interface, composed of a polymer with -$CHO_2(CH_2)_2$-) and -SO_2-Li side groups, GO nanosheets, and LiF.

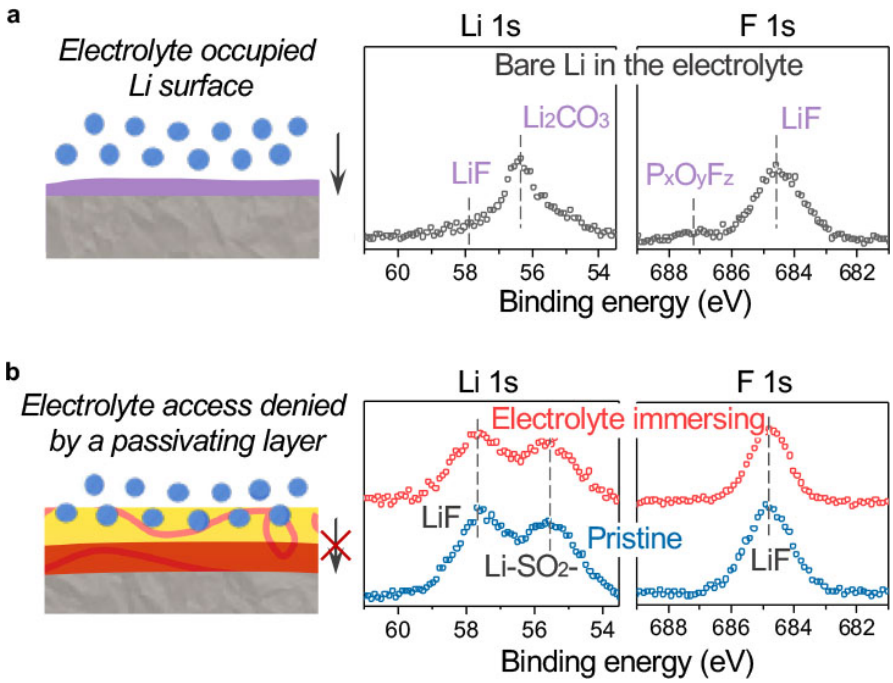

Supplementary Figure 12 | XPS spectra acquired on a bare Li surface immersed in the electrolyte (a) and RPC-stabilized Li surfaces before (blue curves) and after (red curves) immersed in the electrolyte (b). A passivating layer formed by RPC can block the electrolyte access to the Li surface.

As shown in Supplementary Fig. 12a, when contacting with Li, the electrolyte molecules generate LiF (684.8 and 57.6 eV in the F 1s and Li 1s spectra, respectively), Li_2CO_3 (56.2 eV in the Li 1s spectrum), etc. on the fresh Li surface. On the surface of RPC-coated Li, we observed the signals of LiF and -SO_2-Li (55.6 eV in the Li 1s spectrum) groups. No change in the peaks was observed before (blue curves) and after (red curves) the contact with electrolyte, indicating no electrolyte access to the Li surface (Supplementary Fig. 12b). It is worth noting that a highly reactive group is crucial in this surface passivation process since insufficient reactivity will lead to a partial surface coverage[5].

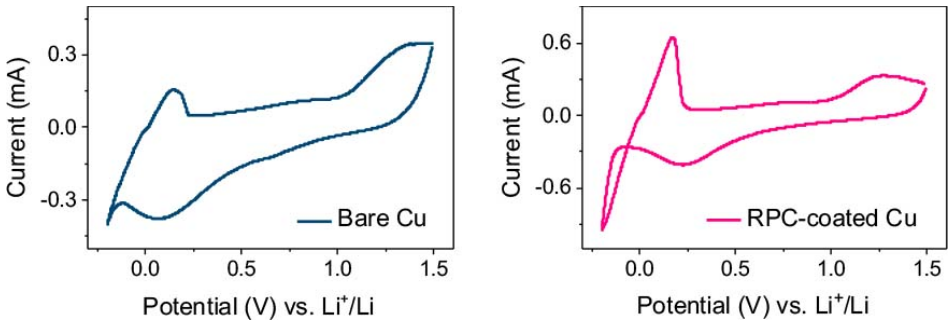

Supplementary Figure 13 | Cyclic voltammetry test of Cu electrodes with and without the RPC coating. The RPC reductively decomposes irreversibly at low potentials. The decomposition peak shift between bare Cu (left curve in blue) and RPC-coated Cu (right curve in pink) in a carbonate electrolyte samples implies the formation of a chemically different SEI from the electrolyte-derived one.

When using a bare Cu as the working electrode, a peak associated with electrolyte-derived SEI formation was detected from 0.25 to -0.12 V vs. Li/Li^+. When applying an RPC-coated Cu as the working electrode, the SEI formation peak shifted by ~0.18 V in the positive direction. Besides, the Li stripping signal of the RPC-stabilized Cu is more intense than that of the bare Cu, indicating that more active Li can strip out after the Li plating. These CV results imply that the formation of an SEI that is chemically different from the electrolyte-derived SEI.

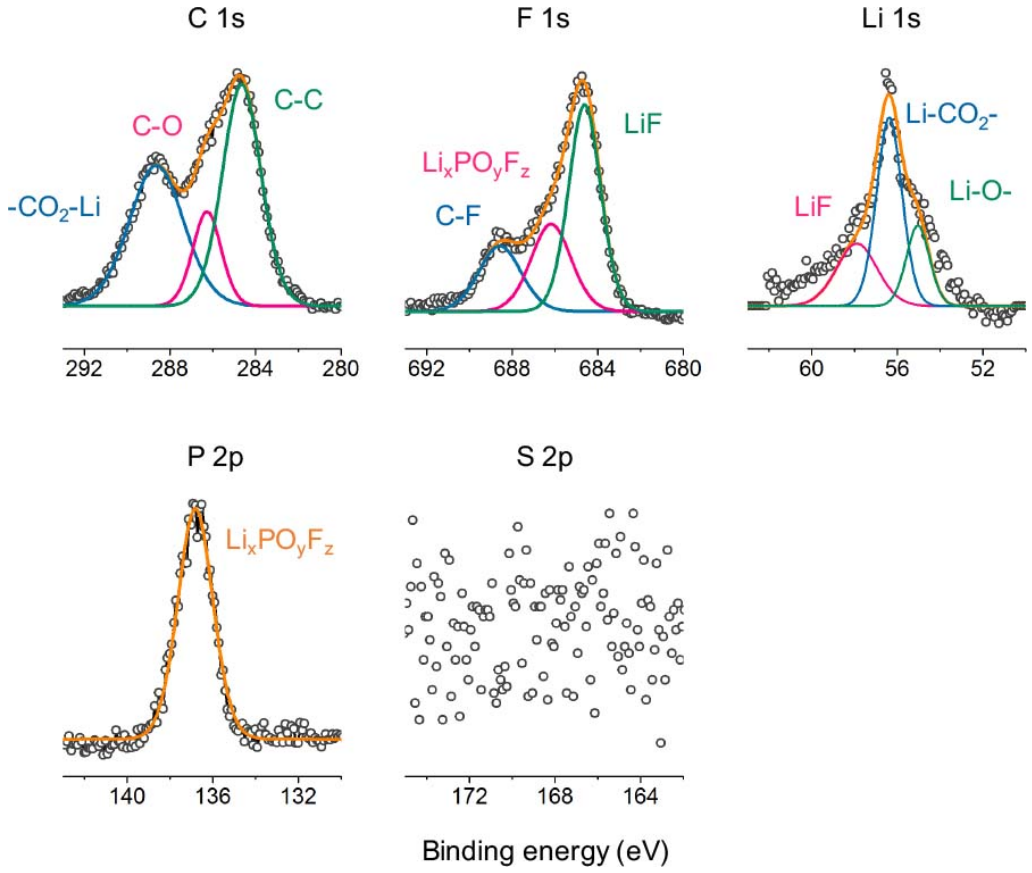

Supplementary Figure 14 | High-resolution XPS spectra of the SEI derived from a carbonate electrolyte.

Supplementary Fig. 14 displays high-resolution C 1s, F 1s, Li 1s, P 2p and S 2p XPS spectra of the carbonate electrolyte-derived SEI. The peak at 289.1 eV in the C 1s spectrum and the peak at 56.2 eV in the Li 1s spectrum can be assigned to Li carbonate salts such as Li-CO_2-OR and Li-CO_2-R (R=hydrocarbons). The peak at 286.2 eV is attributed to the C-O bond, which shows a low concentration in the SEI. The peak at 684.5 eV in the F 1s spectrum and 57.9 eV in the Li 1s spectrum are corresponding to LiF. The peaks at 686.2 eV in the F 1s spectrum and 136.8 eV in the P 2p spectrum can be assigned to $Li_xPO_yF_z$[6]. Overall, the carbonate-based SEI is mainly composed of inorganic Li salts including Li_2CO_3, $Li_xPO_yF_z$, Li_2O, LiF, $LiCO_2R$, etc.

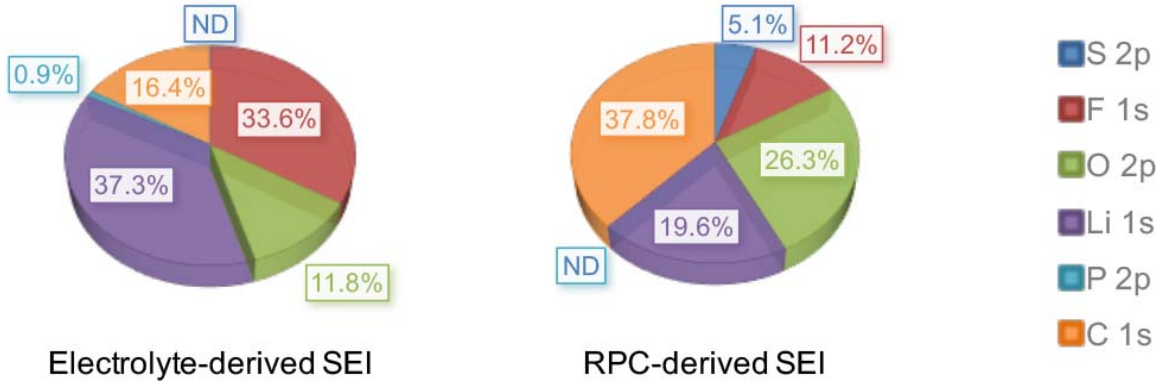

Supplementary Figure 15 | Elemental concentrations of S, F, O, Li, P, and C in the electrolyte-derived SEI and RPC-derived SEI.

The electrolyte-derived SEI presents a high-concentration of Li and F elements since it is mainly composed of inorganic Li salts including Li_2CO_3, $LiP_xO_yF_z$, Li_2O, LiF, $LiCO_2R$, etc. In contrast, the RPC-derived SEI contains a high concentration of C and O elements. This is attributed to the high-content C and O in the RPC.

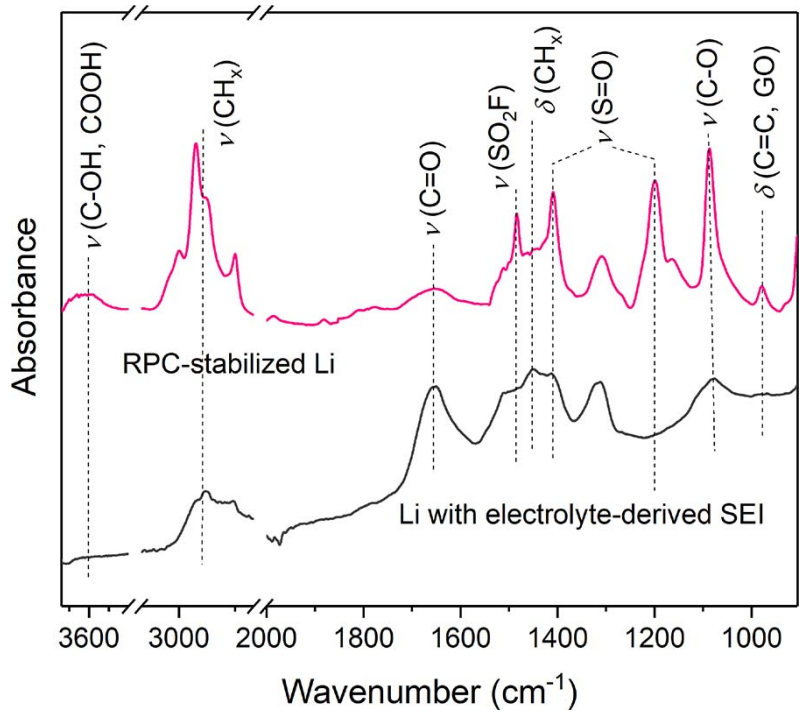

Supplementary Figure 16 | FT-IR spectra of the cycled bare Li (black) and RPC-stabilized Li (red) anodes.

Supplementary Fig. 16 shows the FT-IR analysis of the cycled RPC-stabilized Li (pink line) and bare Li anodes (gray line). In the spectrum of the RPC-stabilized Li, the νSO_2-F/SO_2-Li signal was detected at 1482 cm^{-1}. νS=O signals were observed at 1409 cm^{-1} and 1198 cm^{-1}, respectively. νCOOH and νC-OH of GO nanosheets were found at 3601 cm^{-1}. δC=C (GO) was detected at 977 cm^{-1}. Compared to the electrolyte-derived SEI, the concentrations of C-H_x (2937 cm^{-1}) and C-O (1087 cm^{-1}) are much higher, indicating that the RPC-stabilized Li surface contains much higher organic species, which comes from the unreacted RPC and the RPC-derived SEI. In the electrolyte-derived SEI, the concentration of the C=O bond, corresponding to the electrolyte decomposition products constitute the SEI.

3. Nanostructure and mechanical strength of the RPC-derived SEI layer

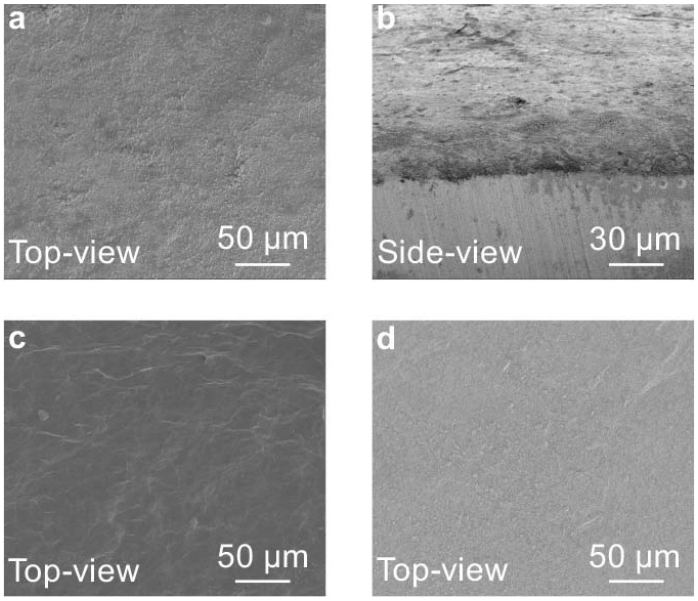

Supplementary Figure 17 | SEM images of the cycled RPC-stabilized Li. a,b, Top- and side-view SEM images of the RPC-stabilized Li after 100 cycles. **c,d,** SEM images of the RPC-stabilized Li after 20 (**c**) and 50 (**d**) cycles with a deposition capacity of 2.0 mAh cm^{-2}. All Li electrodes were prepared by cycling a Li|Li symmetric cell in a 1 M $LiPF_6$ in EC: EMC: FEC (3:7:1, v/v/v) electrolyte for 10 cycles. The Li plating/stripping amount is 1.0 mAh cm^{-2}.

Supplementary Fig. 17a,b shows the morphology of the cycled RPC-stabilized Li after 100 cycles in a carbonate electrolyte. The Li deposition amount is 1.0 mAh cm^{-2}. Supplementary Fig. 17c,d showed the morphology of the cycled RPC-stabilized Li after 20 and 50 cycles, respectively. The Li deposition amount is 2.0 mAh cm^{-2}. The top surface of the electrode was covered by the unreacted RPC layer, and no Li dendrites were observed.

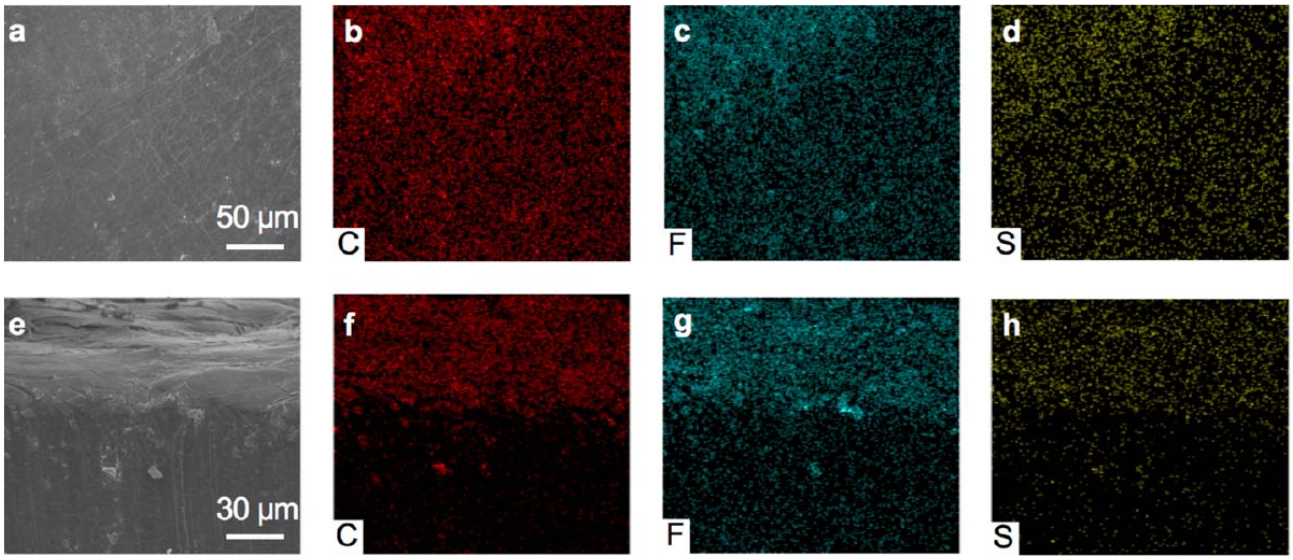

Supplementary Figure 18 | Elemental mapping of the RPC-derived SEI. a-d, Elemental mapping images of C, F, and S based on **a** (top view). **e-h**, Elemental mapping images of C, F, and S based on **e** (side view).

Supplementary Fig. 18 displays elemental mapping images of C, S, and F based on the top- and side-view images. C, S, and F elements are uniformly distributed on the top surface of the electrode, indicating the good integrity of the RPC. This result is consistent with our hypothesis that Li can electrochemically plate underneath the RPC, and the RPC with its micro-scale thickness acts as a "buffering layer" to tolerate the interfacial fluctuation and surface morphology changes of Li and to continue generating the stable SEI on the Li surface.

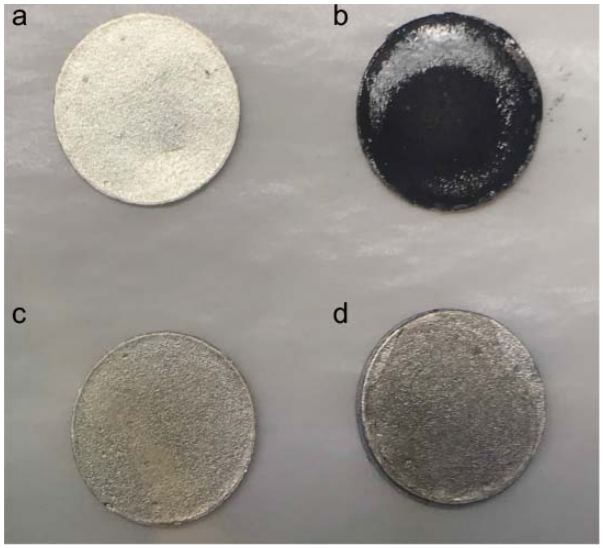

Supplementary Figure 19 | Optical photographs of the RPC-stabilized Li before and after cycling. a,**b**, Bare Li electrodes before (**a**) and after (**b**) cycling. **c**,**d**, The RPC-stabilized Li electrodes before (**c**) and after (**d**) cycling. The electrodes were cycled with an areal capacity of 1.0 mAh cm^{-2} at the current density of 1.0 mA cm^{-2} and for 30 cycles.

The cycled bare Li turns black and rough after cycling. The black species can be assigned to dead Li and accumulated SEI. In contrast, the cycled RPC-stabilized Li presents a flat surface, and the yellow RPC coating was observed on the surface.

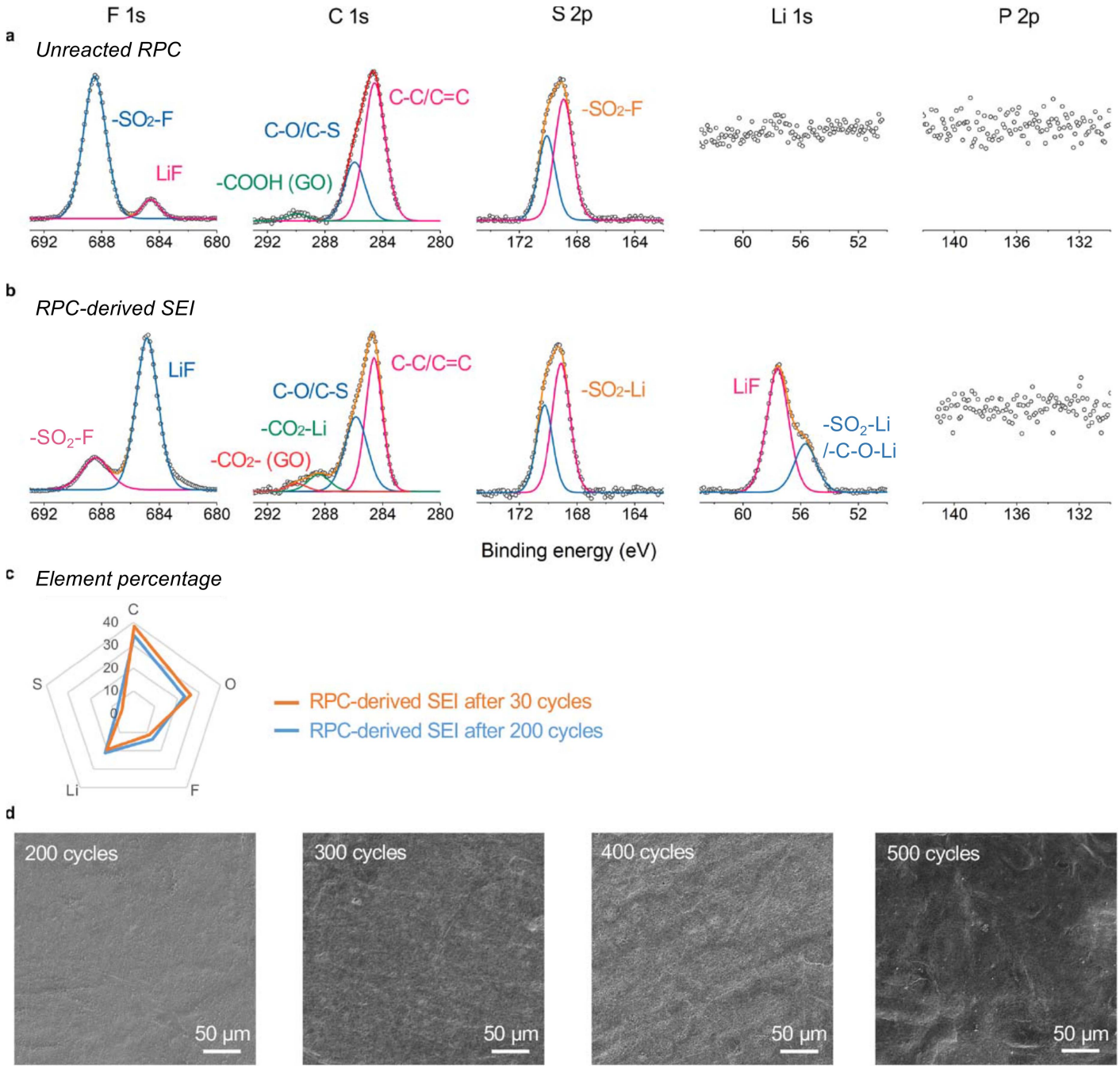

Supplementary Figure 20 | Chemical and physical evolution of the RPC-stabilized Li during long cycling. **a**,**b**, High-resolution XPS spectra of the unreacted RPC (**a**) and RPC-derived SEI (**b**) after 200 cycles. The unreacted RPC retains the chemical structure of pristine RPC. The RPC-derived SEI mainly consists of a polymer integrating side groups of -SO_2-Li, -C-O-Li, and -SO_2-F, inorganic Li salts (LiF and LiOR), and GO nanosheets. **c**, Comparison of the elemental concentrations of the RPC-derived SEI after 30 (orange line) and 200 (blue line) cycles. These two RPC-derived SEI layers show highly consistent concentrations of C, O, Li, F, and S elements. **d**, SEM images of the surface of the RPC-stabilized Li electrodes after 200, 300, 400, and 500 cycles. The RPC-stabilized Li electrodes were cycled in a 1 M $LiPF_6$ in EC/EMC/FEC electrolyte. The Li plating/stripping amount for each cycle is 1.0 mAh cm^{-2}.

We have examined the compositional and morphological evolution of the RPC-stabilized SEI using high-resolution XPS and SEM studies. The XPS spectra of the unreacted RPC and RPC-derived SEI after 200 cycles are shown in Supplementary Fig. 20a,b, respectively. The unreacted RPC layer presents consistent peaks with the pristine RPC (Supplementary Fig. 5d), which include -SO_2-F groups (688.3, 169.4, and 170.6 eV in the F 1s and S 2p spectra, respectively), C-O-C/C-S bonds (286.2 eV in the C 1s spectrum), and -CO_2- groups from GO (289.8 eV in the C 1s spectrum). This indicates that the chemical structure of the unreacted RPC layer is unaltered after long cycles. Meanwhile, the XPS spectra of the RPC-derived SEI after 200 cycles is also consistent with that of the SEI after 30 cycles (Fig. 2c). Peaks at 684.6 and 688.6 eV in the F 1s spectrum are attributed to LiF and -SO_2-F, respectively; split peaks at 170.2 and 169.0 eV in the S 2p spectrum are assigned to overlapped -SO_2-F and -SO_2-Li groups; peaks at 57.6 and 55.6 eV in the Li 1s spectrum are assigned to Li-F and -SO_2-Li/-C-O-Li bonds, respectively; peaks at 289.9, 288.4, 285.9, and 284.6 eV in the C 1s spectrum belong to -CO_2- from GO, -CO_2-Li from reduced GO and the carbonate electrolyte, C-O and C-S bonds (overlapped) from reduced DOL and -SO_2- groups, and C-C bonds from the polymer backbone, respectively; No signals were observed in the P 2p spectrum. There are only slight changes in the position and relative intensity of these peaks, implying good durability of the RPC-derived SEI during cycling. Meanwhile, -CO_2-Li is a representative component (Supplementary Fig. 14 the peak at 289.1 eV in the C 1s spectrum) of the carbonate electrolyte-derived SEI. As shown in Fig. 2c, the concentration of -CO_2-Li groups in the RPC-derived SEI after 30 cycles is very limited. Encouragingly, the -CO_2-Li concentration in the RPC-derived SEI after 200 cycles is similar to that of the SEI after 30 cycles. This result indicates that the RPC-derived SEI remains passive and durable after 200 cycles and continuously prevents the electrolyte decomposition on the Li surface. In addition, XPS elemental concentration analysis reveals that the SEI layers after 30 and 200 cycles have very similar concentrations of C, O, Li, F, and S elements in the SEI (Supplementary Fig. 20c). We also studied the morphology evolution of the RPC-stabilized Li electrodes after 200, 300, 400, and 500 cycles. As shown in Supplementary Fig. 20d, these Li electrodes present flat and Li dendrite-free morphologies and unreacted RPCs were attached on the surface. Collectively, these results demonstrate that the RPC-stabilized Li show stable chemical composition and morphology during long cycling.

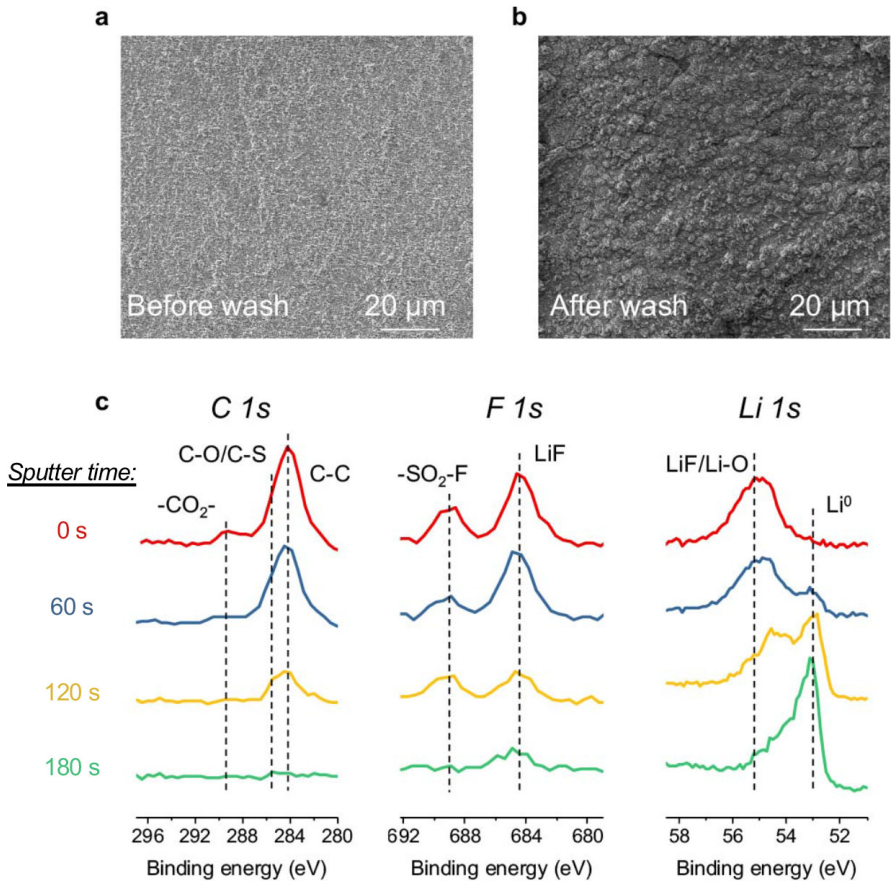

Supplementary Figure 21 | Observation of Li deposition morphology underneath the unreacted RPC layer. a, SEM image of a cycled Li anode with unreacted RPC layer on the top surface. **b**, SEM image of the same piece of Li anode with exposed deposited Li on the top surface. The unreacted RPC layer was removed by DMF wash. **c**, Depth-profiling XPS spectra acquired after sputtering for 0, 60s, 120s, and 180s of a cycled Li anode with exposed deposited Li on the top surface (corresponding to **b**). The sputtering rate is ~10 nm min^{-1} (calculated based on a SiO_2).

We have examined the morphology of Li deposition underneath the unreacted RPC layer. By removing the unreacted RPC layer by washing the cycled Li electrodes with DMF solvent, we can expose the surface of deposited Li and observe the morphology using SEM. As shown in Supplementary Fig. 21a, the Li electrode surface after 200 cycles is flat and covered by an unreacted RPC layer. After DMF wash, the deposited Li coated with RPC-derived SEI was exposed (Supplementary Fig. 21b). The Li plates and strips a dense and dendrite-free manner, which is enabled by RPC-derived SEI. To confirm the removal of unreacted RPC layer, we performed XPS depth profiling on the cycled Li electrode after DMF wash (Supplementary Fig. 21c). LiF (peaks at ~684 eV in the F 1s spectrum and ~56 eV in the Li 1s spectrum), Li-O (the peak at ~55 eV in the Li 1s spectrum), -SO_2-F (the peak at ~689 eV in the F 1s spectrum), C-C (the peak at ~285 eV in the C 1s spectrum), C-O/C-S (the peak at ~286 eV in the C 1s spectrum), and -CO_2- (the peak at ~289 eV in the C 1s spectrum) were observed in the top surface curves. These peaks correspond to the components of the RPC-derived SEI layer, indicating the removal of the unreacted RPC layer on the surface. After sputtering for 3 min, we observed a tiny amount of LiF (peaks at ~684 eV in the F 1s spectrum and ~56 eV in the Li 1s spectrum) and large amount of metallic Li (the peak at ~53eV in the Li 1s spectrum), indicating that the SEI residue layer is also very thin (~30 nm) after DMF wash.

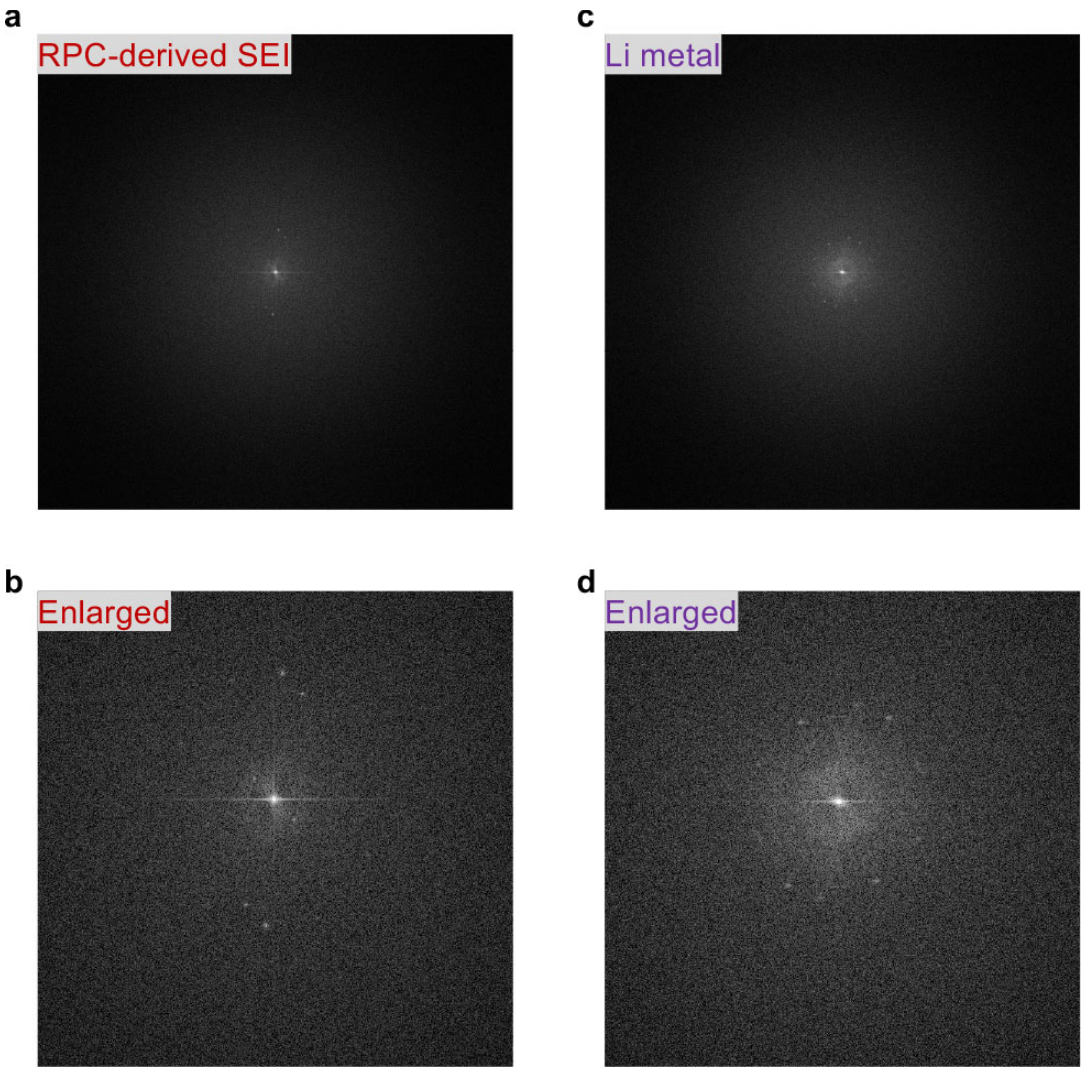

Supplementary Figure 22 | FFT images of the RPC-derived SEI (left) and Li (right) regions taken from the interface of the RPC-stabilized Li.

We measured the lattice spacing using the corresponding FFT images. Supplementary Fig. 22 depicts the corresponding FFT images of the Li (Fig. 3h) and RPC-derived SEI (Fig. 3i) regions taken from the interface of the RPC-stabilized Li. Despite the insufficiently clear TEM images, we can clearly see the presence of LiF lattice in the FFT image corresponding to Fig. 3i (Supplementary Fig. 22a,b) and Li metal lattice in the FFT image corresponding to Fig. 3h (Supplementary Fig. 22c,d) The measured lattice spacings of 0.20 and 0.23 nm are consistent with the {200} and {111} LiF planes, respectively. Other salts (-C-O-Li, -SO_2-F, and -SO_2-Li) connected to the polymer present an amorphous morphology. Li_2CO_3 was not detected in the RPC-derived SEI.

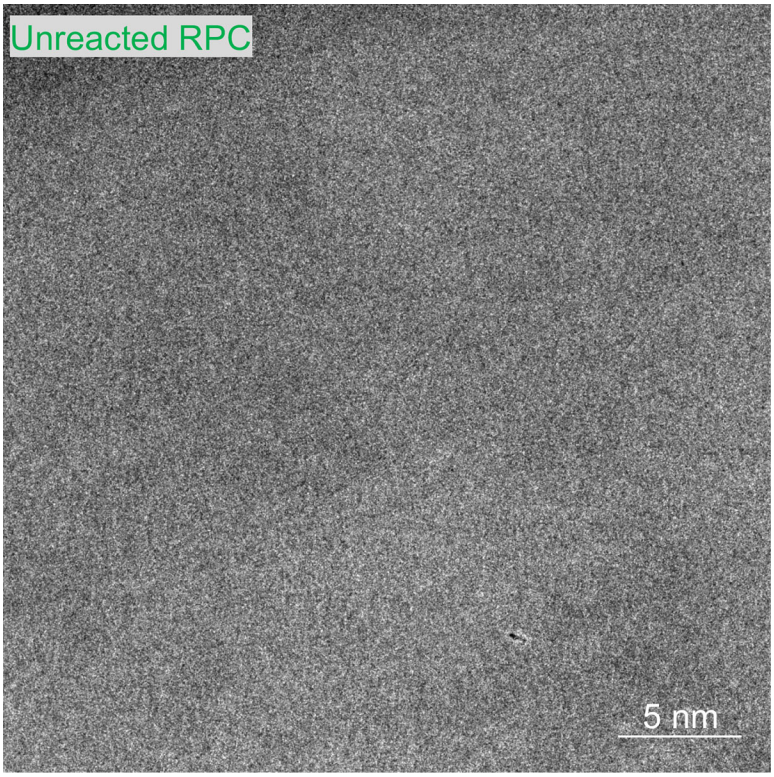

Supplementary Figure 23 |The high-resolution TEM image of the unreacted RPC region taken from the interface of the RPC-stabilized Li.

Supplementary Fig. 23 depicts a high-resolution TEM image of the unreacted RPC region taken from the RPC-stabilized Li in Fig. 3g. The unreacted RPC presents an amorphous majority phase embedded with GO nanosheets.

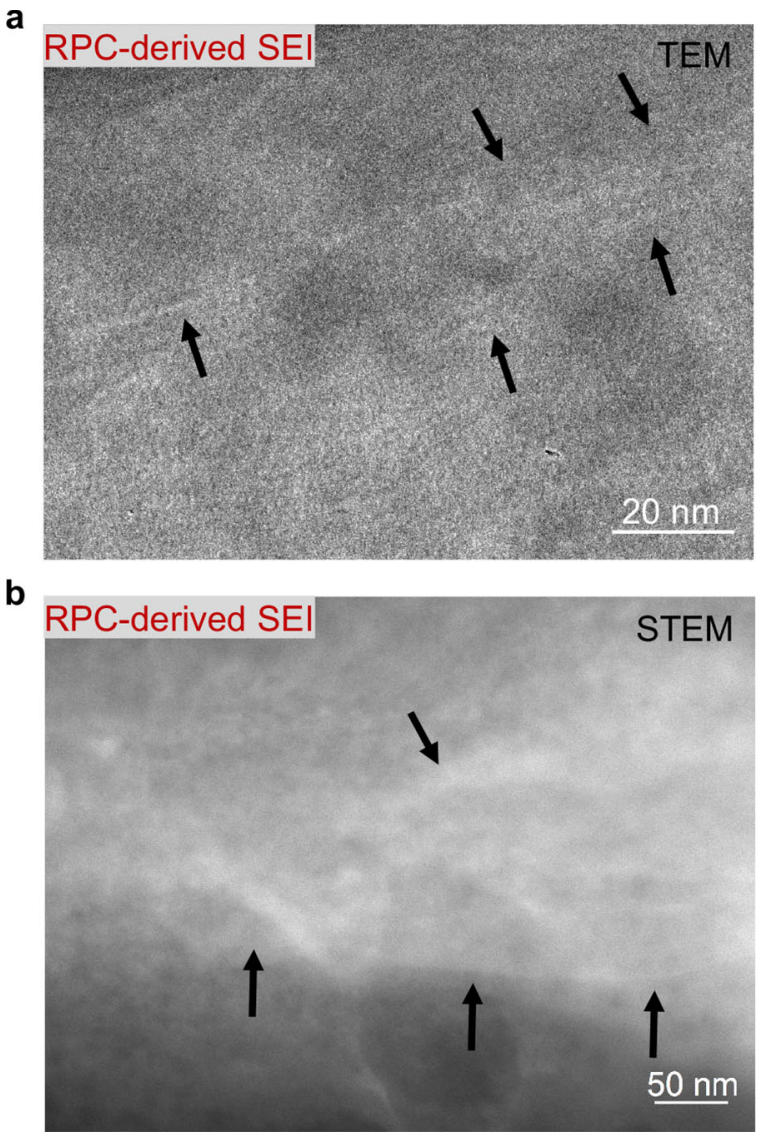

Supplementary Figure 24 | TEM and STEM images of the RPC-derived SEI regions taken from the interface of the RPC-stabilized Li.

Supplementary Fig. 24 displays TEM and STEM images of the RPC-derived SEI regions taken from the interface of the RPC-stabilized Li. Under the relatively low magnification, we observed some wavy areas (as indicated by the arrows) in the RPC-derived SEI, which are probably the GO nanosheets in the SEI. The polymer-GO nanosheet structure leads to good density of the SEI layer and the RPC material.

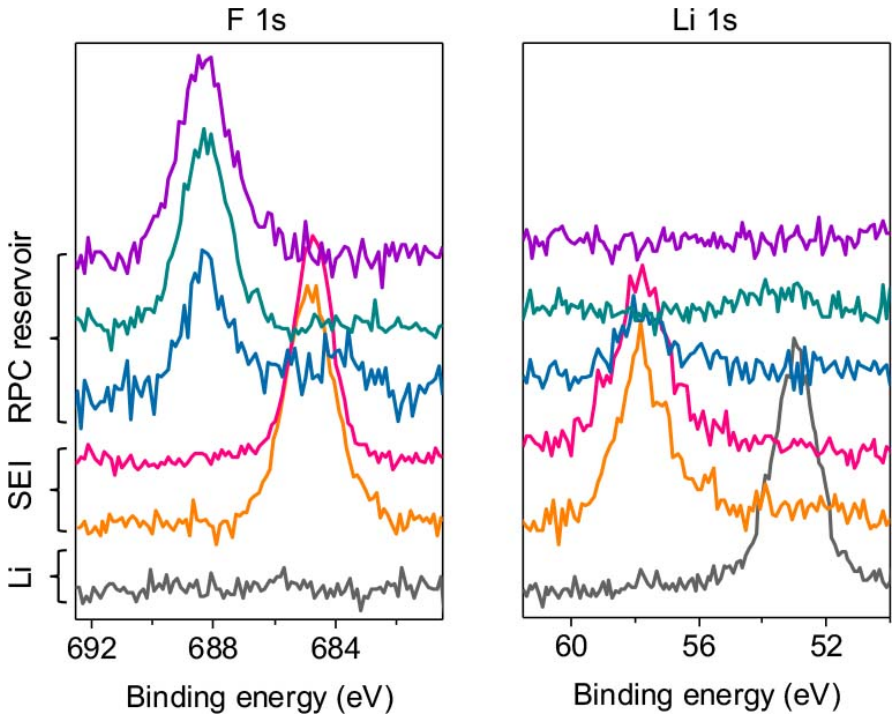

Supplementary Figure 25 | XPS depth profiling of the cycled RPC-stabilized Li.

We conducted XPS depth profiling on the surface of the cycled RPC-stabilized Li. Li and F were selected as the signature elements for structural identification (Supplementary Fig. 25). The top two curves (purple and green lines) present the -SO_2-F signal (peaks at 688.3 eV in the F 1s spectrum) and show no Li signal, and thus can be assigned to the unreacted RPC. The 3rd curve (blue line) contains both the -SO_2-F signal from the unreacted RPC and Li salts signals (peaks at 684.8 eV in the F 1s spectrum and 57.8 eV in the Li 1s spectrum), which correspond to the RPC-derived SEI. The middle two curves (pink and orange lines) present Li salt signals, which is the SEI layer. The bottom curve in grey contains the metallic Li signal (peaks at 53.2 eV in the Li 1s spectrum) and has no F signal, which can be attributed to metallic Li.

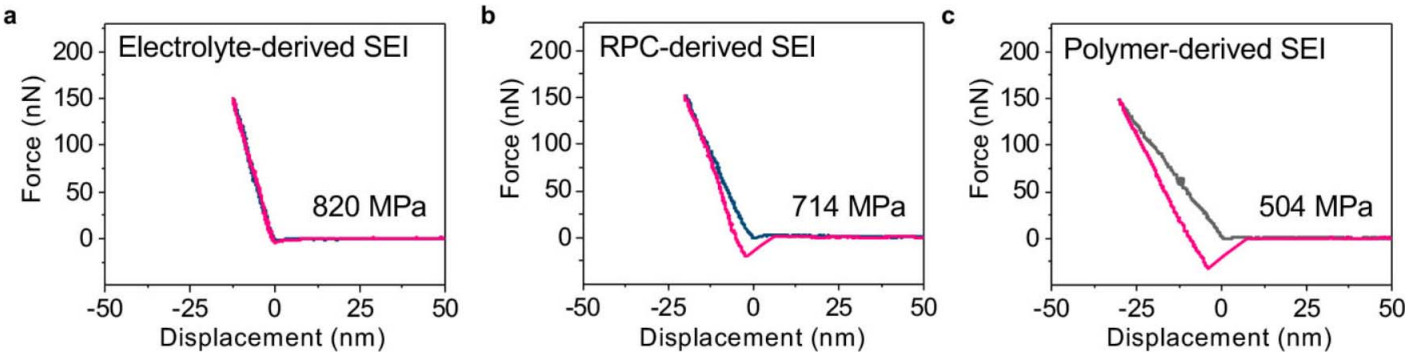

Supplementary Figure 26 | Force-displacement plots of the electrolyte-derived SEI (a), RPC-derived SEI (b), and polymer-derived SEI (c).

To investigate the effect of SEI mechanical strength, we compared the modulus of electrolyte-derived SEI, RPC-derived SEI without GO, and RPC-derived SEI, which were measured by AFM indentation[7,8]. The electrolyte-derived SEI shows loading and unloading curves overlapping with little hysteresis (Supplementary Fig. 26a), and the calculated modulus based on the Oliver-Pharr model is 820 MPa (Supplementary Fig. 27). This implies that the SEI is brittle and rigid. In contrast, a clear hysteresis between the loading and unloading curves and meniscus dragging during the tip snap-off were observed for RPC-stabilized Li (Supplementary Fig. 26b), and the calculated modulus was 714 MPa, implying good flexibility and stiffness. Interestingly, the P(SF-DOL) polymer-derived SEI without GO displays less elastic behavior than the RPC-derived SEI, which is evidenced by a larger hysteresis between the loading and unloading curves and easier yielding under an applied force. The calculated modulus was 504 MPa (Supplementary Fig. 26c). Correspondingly, a dendrite-free morphology was seen for the cycled Li with this SEI within 50 cycles. Li dendrites were found after 100 cycles (Supplementary Figs 28 and 29).

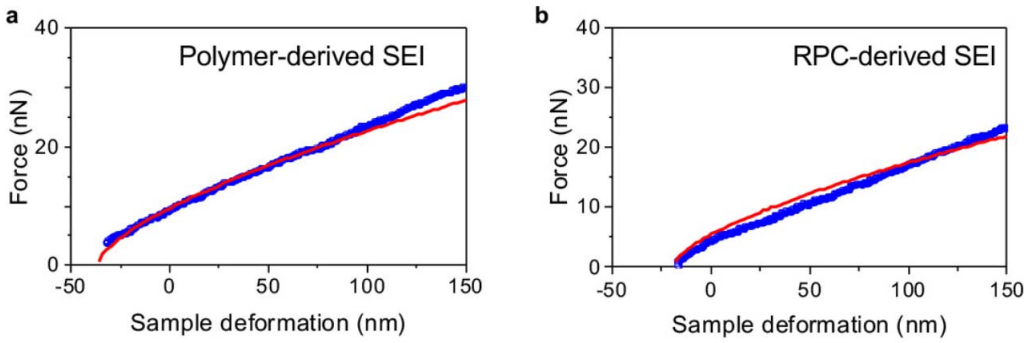

c

Surface Material / fitting model	Oliver-Pharr model (MPa)	DMT model (MPa)
Electrolyte-derived SEI	**820**	Not appropriate
Polymer-derived SEI	**504**	346
RPC-derived SEI	**714**	518
Polymer	460	306
RPC	630	472

Supplementary Figure 27 | Fitting based on Oliver-Pharr and DMT contact models.

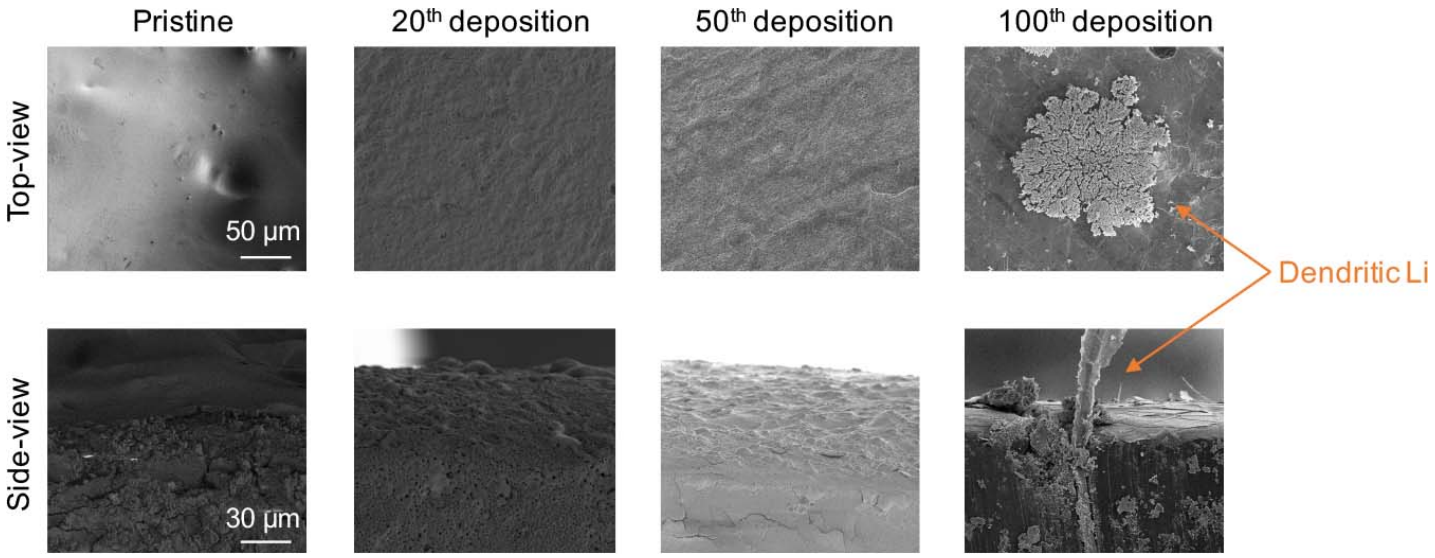

Supplementary Figure 28 | SEM images of the cycled Li with P(SF-DOL) after 50 cycles in a carbonate electrolyte.

Supplementary Fig. 28 shows the morphology of Li with P(SF-DOL) after 50 cycles in a carbonate electrolyte. The pristine Li with P(SF-DOL) presents a flat surface morphology, and a clear surface film can be viewed from the side-view SEM image. After 20 and 50 cycles, the P(SF-DOL) still protects the top surface of the Li electrode. However, Li dendrite penetrates the P(SF-DOL) film after 100 cycles. In contrast, no Li dendrites were found in the SEM images of the RCP-stabilized Li anodes after 100 cycles (Supplementary Fig. 17a,b) and 500 cycles (Supplementary Fig. 20). The possible reasons are that the mechanical strength of the P(SF-DOL)-derived SEI is too poor to tolerate the interfacial fluctuation of Li, leading to some cracks. Therefore, the deposited Li is contacted with the carbonate electrolyte, triggering the Li dendrite growth. In addition, the use of GO nanosheets has been reported to be capable of effectively eliminating the "tip effect" in the Li deposition and leads to more homogeneous Li nucleation[9].

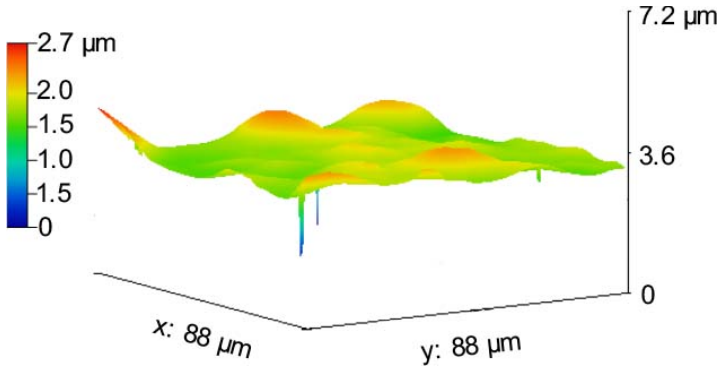

Supplementary Figure 29 | Three-dimensional optical profilometry image of the surface of the cycled Li with P(SF-DOL).

Compared to the cycled bare Li, Li with P(SF-DOL) displays a flat surface morphology. However, the height differences are up to 2.7 µm, which is much larger than that of the RPC-stabilized Li. Some defects were observed on the electrode surface, indicating the inadequate integrity of the polymer.

4. Electrochemical performance of RPC-stabilized metal anodes

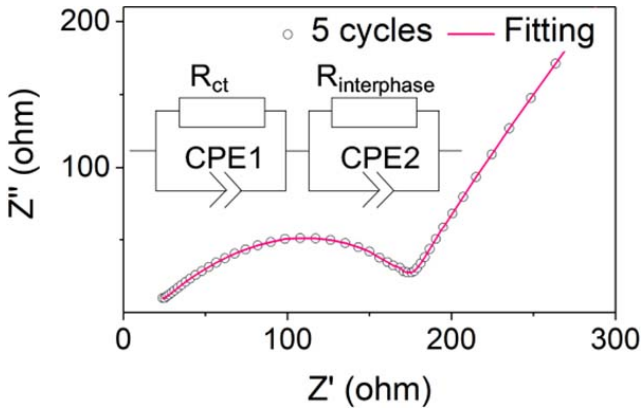

Supplementary Figure 30 | Electrochemical impedance spectroscopy measurement of the RPC-stabilized Li after 5 cycles. The resistance of the RPC coating and RPC-derived SEI ($R_{interphase}$) is ~140 Ω. The area of the Li anode is 2.0 cm^2.

As shown in Supplementary Fig. 30, the resistance of the RPC coating and RPC-derived SEI ($R_{interphase}$) is only ~140 Ω, which is acceptable for battery operation.

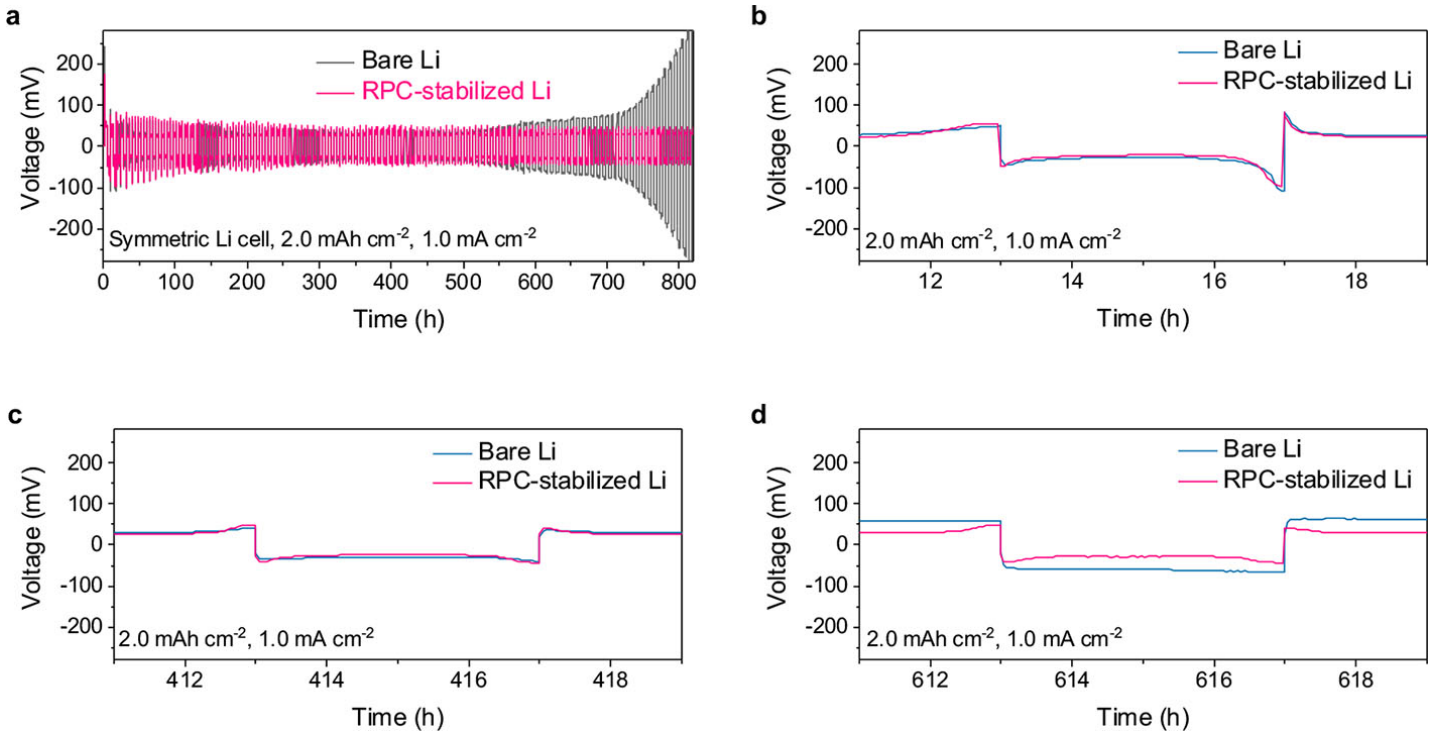

Supplementary Figure 31 | Voltage profiles of a symmetric RPC-stabilized Li cell over 800 h.

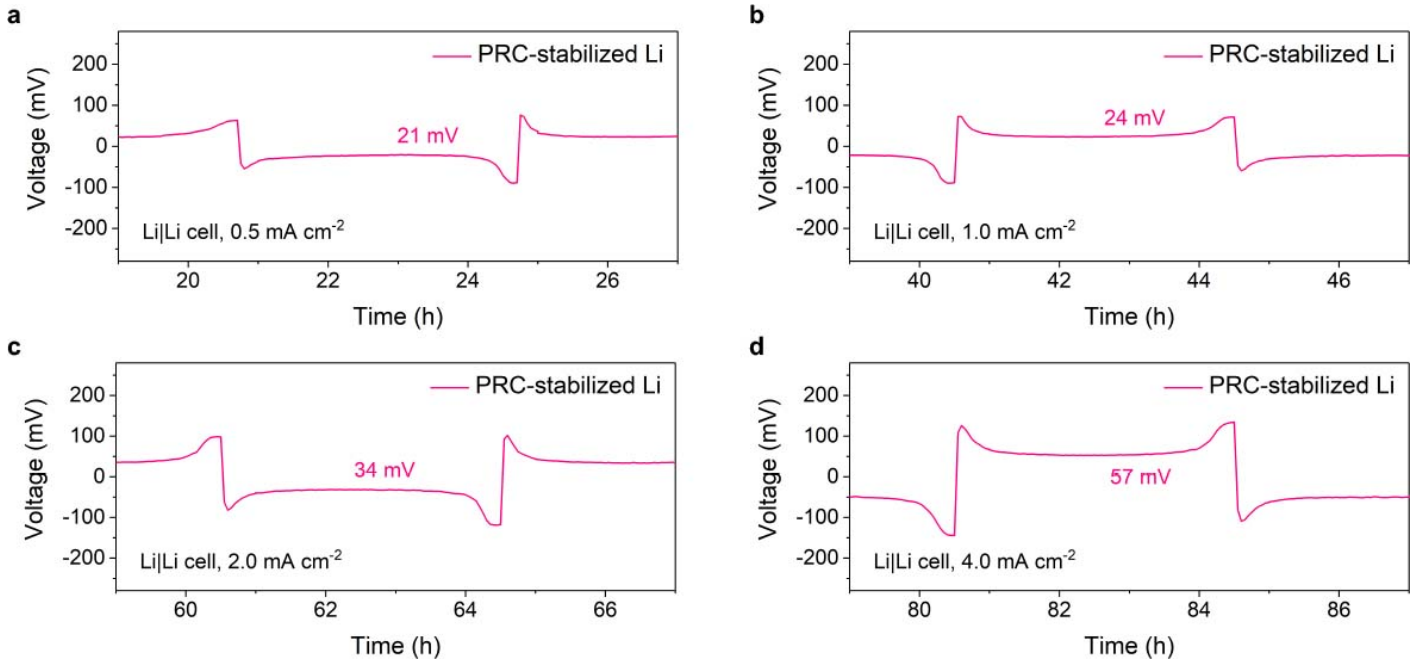

Supplementary Figure 32 | Li deposition overpotentials of the RPC-stabilized Li electrodes at different current densities. The overpotentials of Li deposition are 21, 24, 34 and 57 mV at the current densities of 0.5, 1.0, 2.0, and 4.0 mA cm^{-2}, respectively.

As shown in Supplementary Fig. 32, the Li deposition overpotentials of the RPC-stabilized Li electrodes are 21, 24, 34 and 57 mV at the current densities of 0.5, 1.0, 2.0, and 4.0 mA cm^{-2}, respectively.

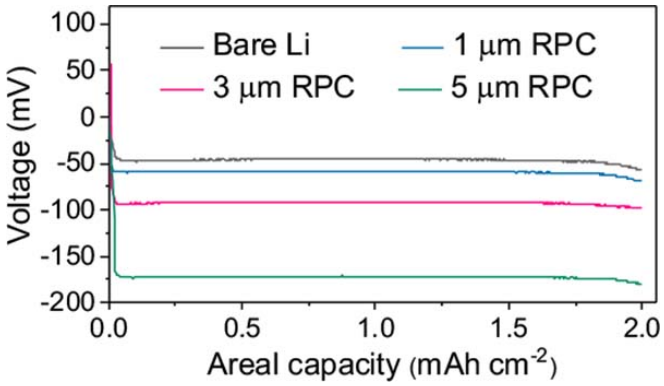

Supplementary Figure 33 | Thickness optimization of the RPC layer. The Li deposition overpotential of the Li electrodes coated with RPC with different thicknesses.

Supplementary Fig. 33 depicts the voltage profiles of the initial Li deposition underneath the RPC at a high current density of 2.0 mA cm^{-2}. An acceptable overpotential of ~90 mV was achieved by controlling the thickness of the RPC at ~3 μm. The thicker one (~5 μm) induces a high deposition overpotential of ~167 mV.

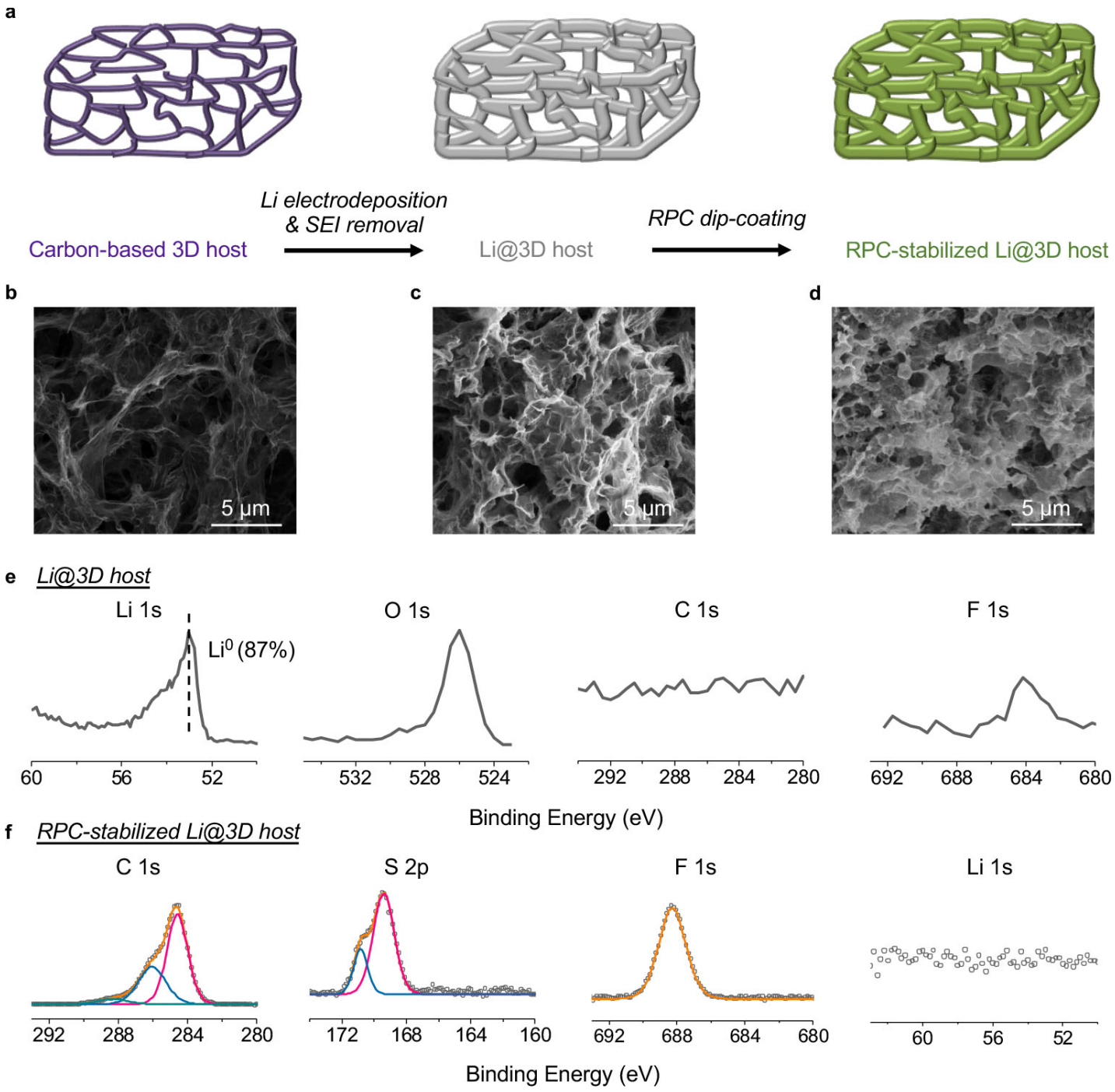

Supplementary Figure 34 | Preparation of RPC-stabilized Li@3D host electrodes. a, Illustration of the preparation process. **b-d**, SEM images of the bare 3D host (**b**), SEI-removed Li@3D host (**c**), and RPC-stabilized Li@3D host (**d**) electrodes. **e**, XPS spectra of the surface of a Li@3D host electrode. The SEI layer generated in the Li deposition step has been removed. **f**, XPS spectra of the surface of an RPC-stabilized Li@3D host electrode. The signals of RPC can be found on the electrode surface.

To prepare the RPC-stabilized Li@3D host electrodes (Supplementary Fig. 34a), we electrochemically deposited a certain amount of Li onto the surface of the host (~1 cm^2) and then removed the SEI generated in the electrodeposition process. After drying the electrode, we coated RPC onto the surface of Li by immersing the Li@3D host electrode into a concentrated solution of P(SF-DOL)-GO. As shown in Supplementary Fig. 34b-d shows the SEM images of the bare carbon-based 3D host, SEI-removed Li@3D host, and RPC-stabilized Li@3D host (from left to right). Li was deposited on the 3D host uniformly. The removal of the SEI layer was confirmed by XPS measurement. We found ~ 87% metallic Li on the surface of the Li@3D host and a small amount of Li_2O (peaks at ~526 eV in the O 1s spectrum and ~55 eV in the Li 1s spectrum) and LiF (peaks at ~684 eV in the F 1s spectrum and ~56 eV in the Li 1s spectrum) (Supplementary Fig. 34e). After being coated with an RPC layer, the surface morphology turned slightly blurred. We confirmed the presence of the RPC layer by XPS as well. The XPS spectra taken from the surface of an RPC-stabilized Li@3D host electrode are consistent with the pristine RPC, including C-C (the peak at 284.6 eV in the C 1s spectrum), C-O/C-S (the peak at 286.3 eV in the C 1s spectrum), $-CO_2-$ (the peak at 289.6 eV in the C 1s spectrum), $-SO_2-F$ (peaks at 688.3 eV in the F 1s spectrum and 169.4 and 170.6 eV in the S 2p spectrum) (Supplementary Fig. 34f). This indicates the successful coating.

The electrochemical deposition of Li onto the surface of the 3D host was conducted in a Li|3D host cell using 4 M lithium bis(fluorosulfonyl) imide in dimethoxyethane electrolyte. 1.0 mAh cm^{-2} was pre-plated onto the 3D host and then stripped out at a current of 0.5 mA cm^{-2}. This process serves as an activation step to pre-form an SEI layer on the 3D host surface. Next, we plated a certain amount of Li (e.g. 3.4 mAh cm^{-2}) onto the 3D host at a current density of 0.5 mA cm^{-2}.

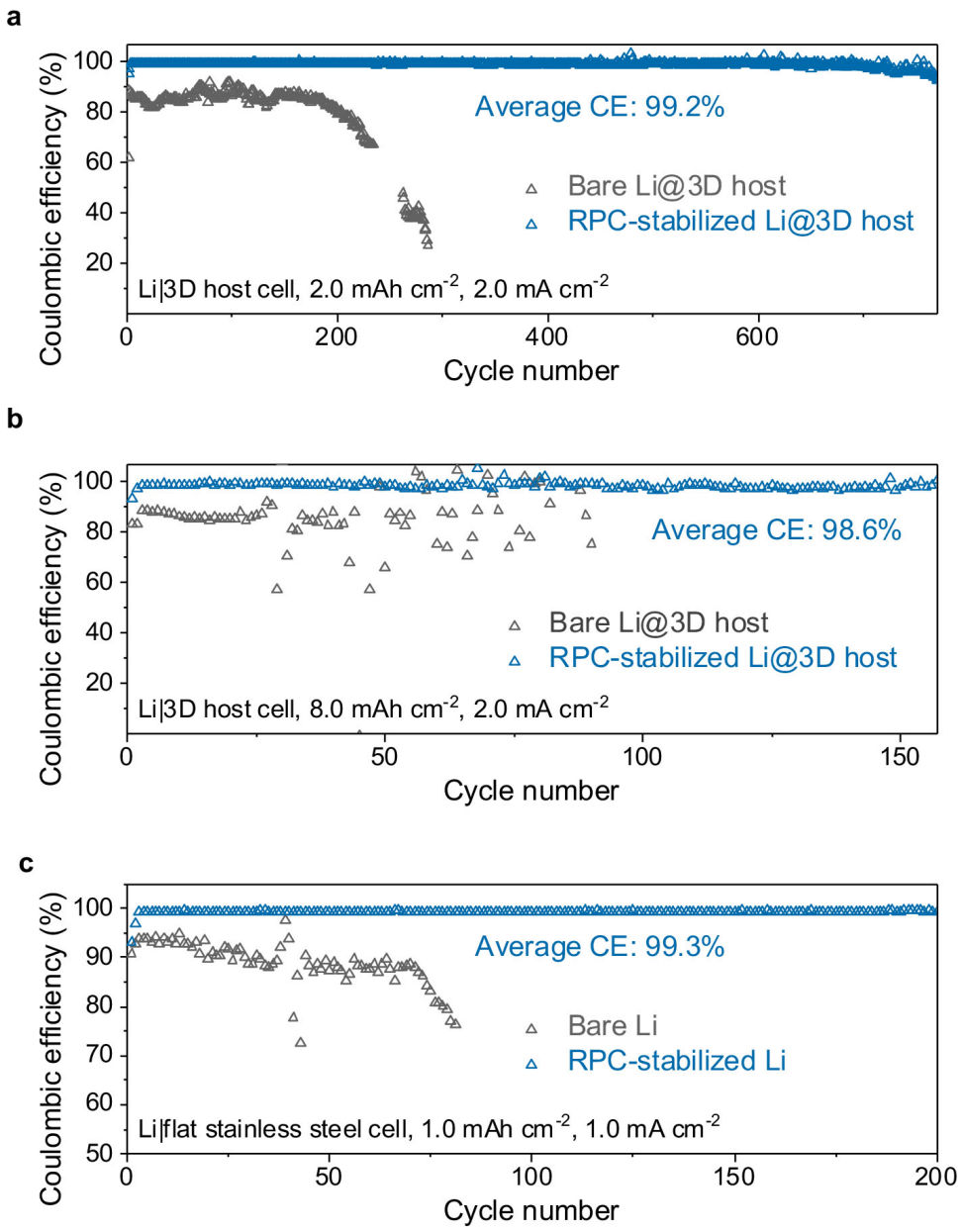

Supplementary Figure 35 | a,b, Efficiencies of Li plating and stripping in the 3D host at a deposition amount of 2.0 (a) and 8.0 (b) mAh cm^{-2}, respectively. c, Efficiencies of Li plating and stripping on a flat stainless steel foil at a deposition amount of 1.0 mAh cm^{-2}. 1 M $LiPF_6$ in EC/EMC with 2% LiBOB electrolyte was used.

To measure the efficiency, we cast an RPC layer on the surface of the stainless steel and pre-plated 1.0 mAh cm^{-2} Li onto the stainless steel foil with a current density of 1.0 mA cm^{-2} and calculated the efficiency by measuring the capacity of stripped Li.

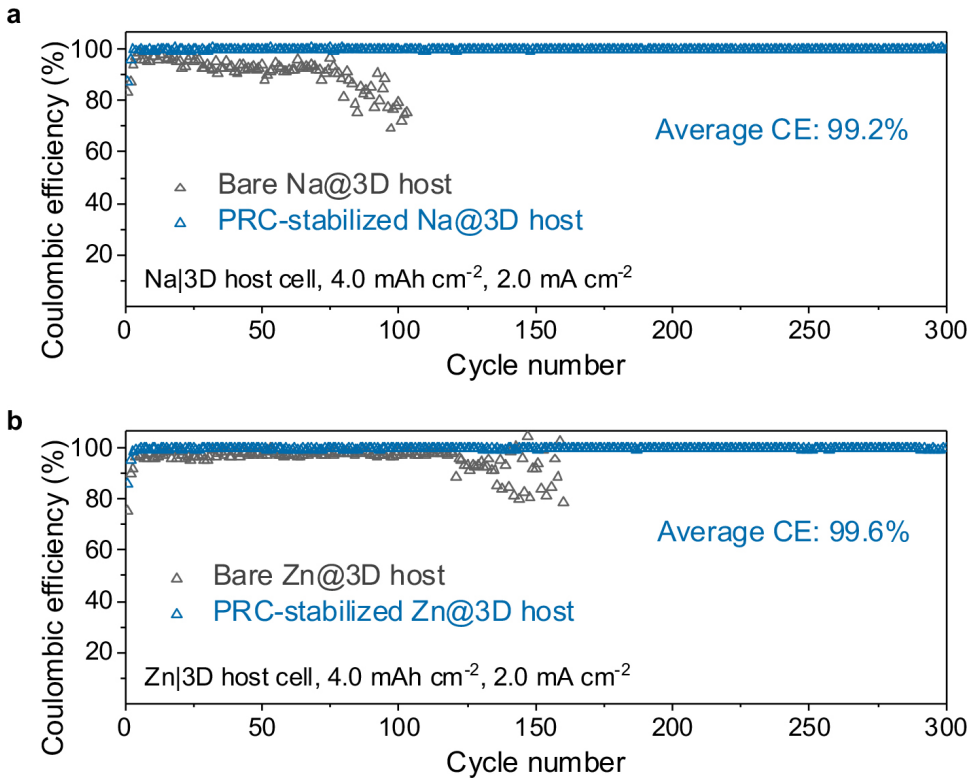

Supplementary Figure 36 | Efficiencies of plating/stripping of Na (a) and Zn (b), respectively, at a deposition amount of 4.0 mAh cm^{-2}.

5. Electrolyte and Li retentions at practical battery operating conditions

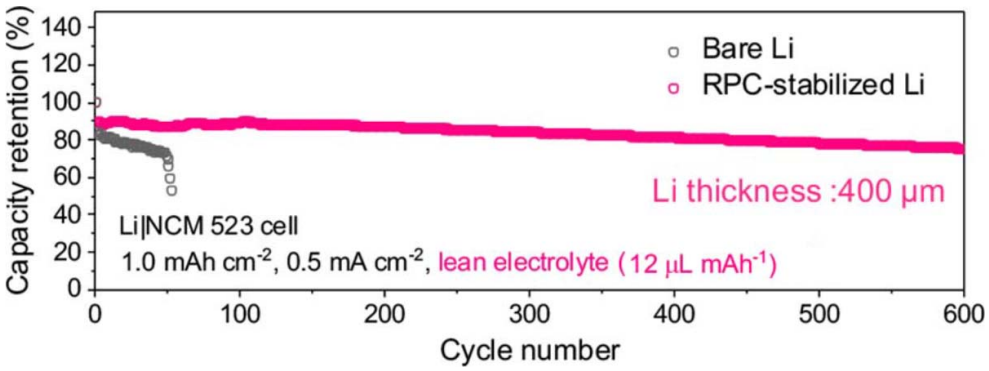

Supplementary Figure 37 | Cycling performance of the Li|NCM 523 cells in the lean electrolytes (1 M $LiPF_6$ in EC/EMC with 2% LiBOB). The electrolyte-to-capacity ratio is 12 μL mAh^{-1}. The Li thickness is 400 μm.

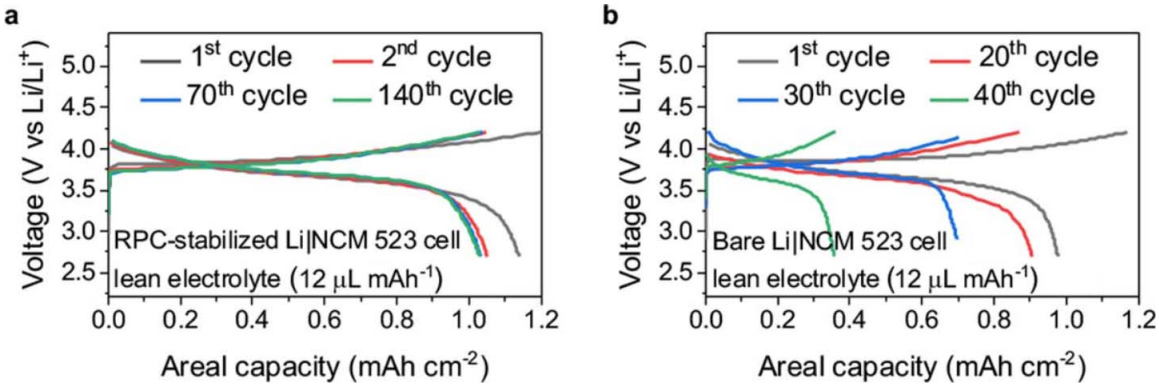

Supplementary Figure 38 | Voltage profiles of the Li|NCM 523 cell under lean electrolyte conditions. a, A cell using the RPC-stabilized Li anode in a lean electrolyte. **b**, A cell using the bare Li anode in a lean electrolyte.

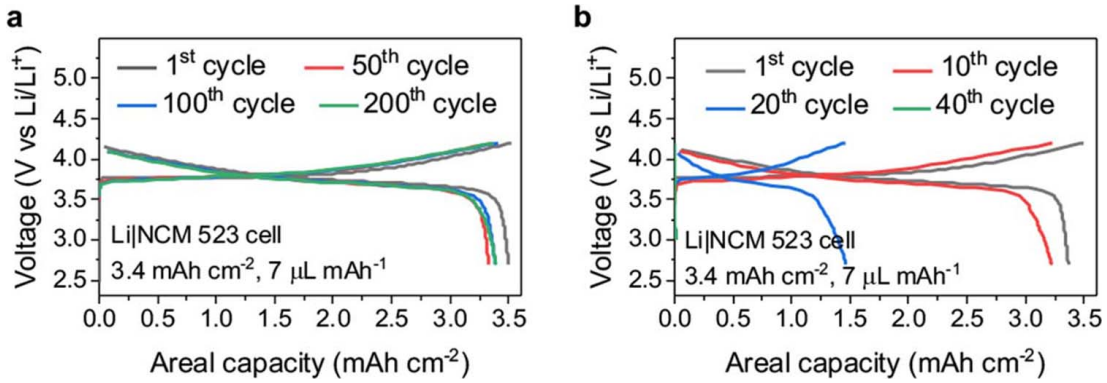

Supplementary Figure 39 | Voltage profiles of the Li|NCM 523 cells incorporating RPC-stabilized Li@3D host anodes under lean electrolyte conditions. a, A cell using the RPC-stabilized Li@3D host anode in a lean electrolyte. **b**, A cell using the bare Li@3D host anode in a lean electrolyte.

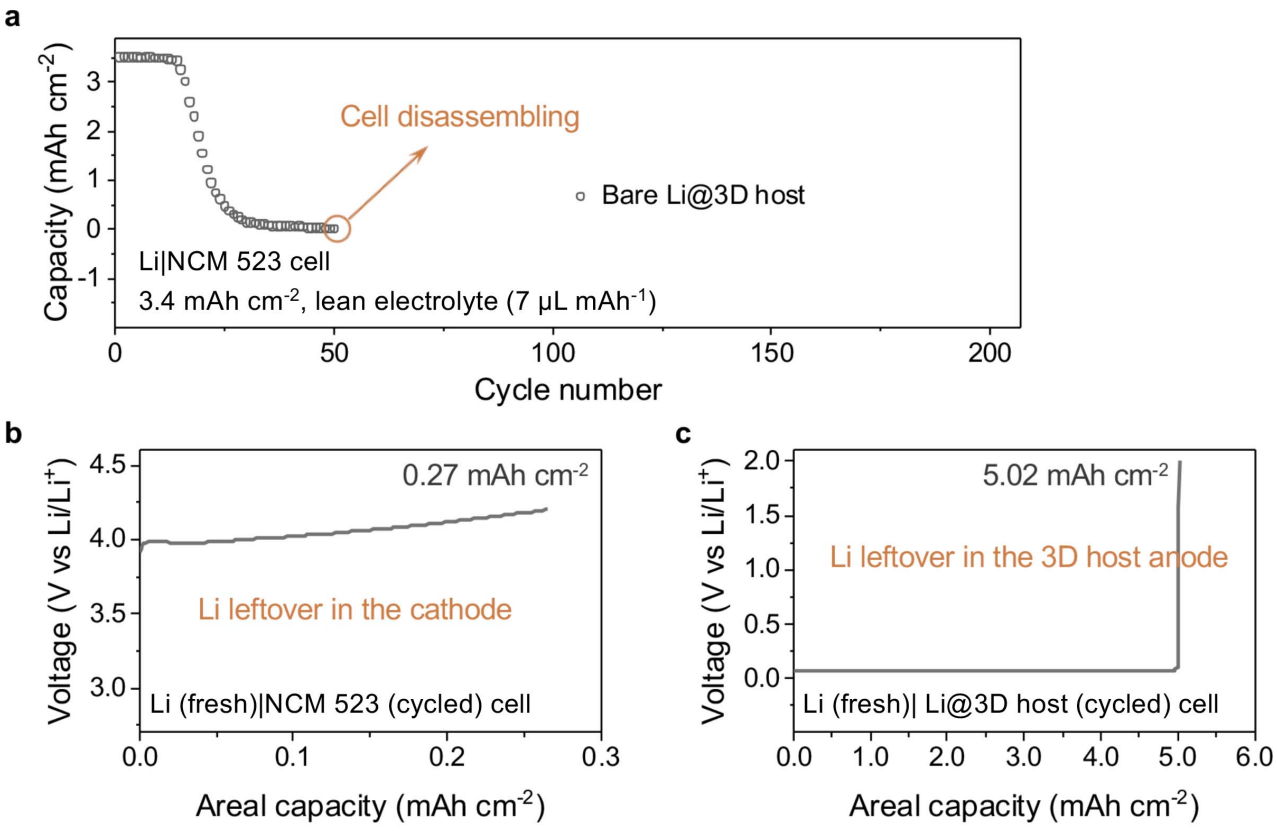

d

Electrode	Li leftover amount	Total amount of Li
Initial NCM 523 cathode	0	10 mAh cm^{-2}
Initial 3D host	10 mAh cm^{-2}	
NCM 523 cathode after 50 cycles	0.27 mAh cm^{-2}	5.3 mAh cm^{-2}
3D host after 50 cycles	5.02 mAh cm^{-2}	

Supplementary Figure 40 | The Li|NCM 523 cell incorporating conventional SEI after 50 cycles, which is used for electrolyte retention studies.

Taking the fabrication of the unprotected Li|NCM 523 cell as an example (Supplementary Fig. 40a), an as-prepared NCM 523 cathode was charged to 4.2 V for delithiation. 10 mAh cm^{-2} active Li were initially stored in the 3D host. These two electrodes were then assembled using a small amount of electrolyte (7 μL mAh^{-1}). After 50 cycles, we disassembled the cell, paired the cycled NCM 523 cathode and 3D host with Li counter electrodes and supplied fresh electrolyte, respectively. We charged the new Li (fresh)|NCM 523 (cycled) cell to 4.2 V, and the cell showed a capacity of 0.27 mAh cm^{-2} (Supplementary Fig. 40b). This means that 0.27 mAh cm^{-2} was left in the cycled NCM 523 electrode. Meanwhile, the 3D host released 5.02 mAh cm^{-2} Li in the delithiation process (Supplementary Fig. 40c). The total Li left over in the NCM 523 cathode and 3D host was 5.3 mAh cm^{-2} (Supplementary Fig. 40d). We therefore determined that 53% of Li was left in the cell after cycling.

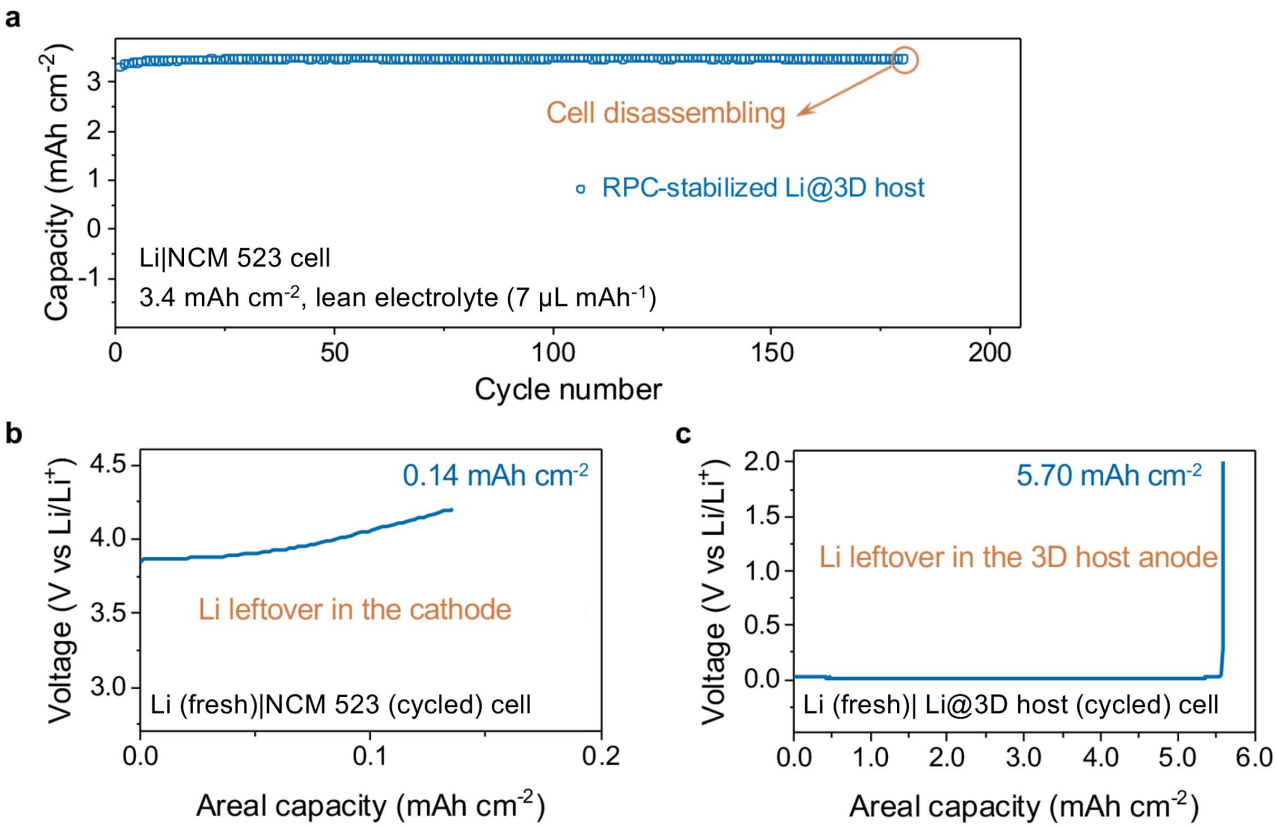

d

Electrode	Li leftover amount	Total amount of Li
Initial NCM 523 cathode	0	10 mAh cm^{-2}
Initial 3D host	10 mAh cm^{-2}	
NCM 523 cathode after 180 cycles	0.14 mAh cm^{-2}	5.8 mAh cm^{-2}
3D host after 180 cycles	5.70 mAh cm^{-2}	

Supplementary Figure 41 | The Li|NCM 523 cell incorporating RPC-derived SEI after 180 cycles, which is used for electrolyte retention studies.

The Li leftover in the protected Li|NCM 523 cell (Supplementary Fig. 41) was measured using the same method described above in the discussion of Supplementary Fig. 40.

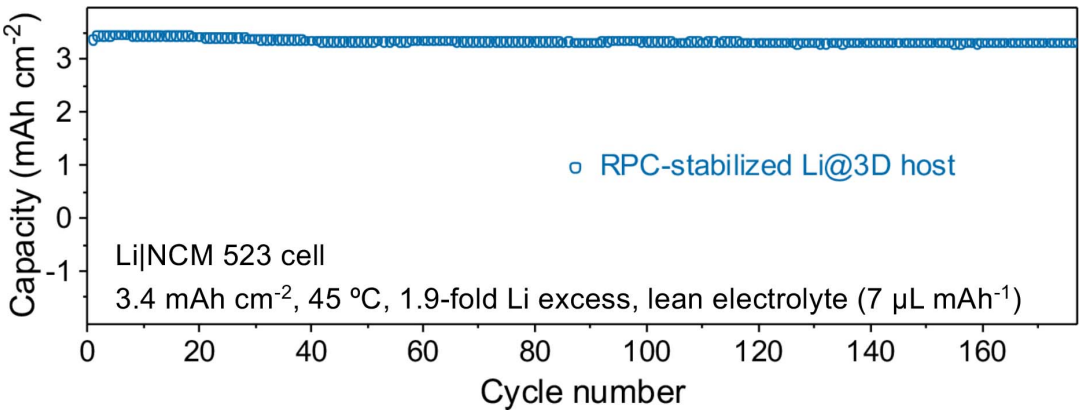

Supplementary Figure 42 | Cycling performance of Li|NCM 523 cells under an elevated temperature (45 ºC). An FEC-free electrolyte (1 M $LiPF_6$ in EC/EMC with 2% LiBOB) was used.

Strategy	Cell design	Cathode capacity	Cyclability	Electrolyte	Electrolyte amount	Li metal thickness	Reference
1. Artificial protective layer	Li|LFP cell	0.5 mAh cm^{-2}	85% CR after 150 cycles	1M $LiPF_6$ in EC/DEC (1:1 vol)	**230 µL mAh^{-1}**	n/a	Nature Commun. 6, 10101 (2015)
2. Li host	Li|LCO cell	0.35 mAh cm^{-2}	~86% CR after 100 cycles	1M $LiPF_6$ in EC/DEC (1:1 vol) +2% VC	**n/a**	27.25 µm (10.9 mAh cm^{-2})	Nat. Nanotechnol. 11, 626 (2016)
3. Artificial protective layer	Li|LTO cell	0.5 mAh cm^{-2}	~80% CR after 1500 cycles	1M LiTFSI in DOL/DME (1:1 vol)	**80 µL mAh^{-1}**	200 µm	Nat. Energy 2, 17119 (2017)
4. Electrolyte engineering	Li|NMC 442 cell	1.5 mAh cm^{-2}	~93% CR after 168 cycles	0.6M LiTFSI + 0.4M LiBOB in EC/EMC (4:6 wt) + 0.05M $LiPF_6$	**67 µL mAh^{-1}**	120 µm	Nat. Energy 2, 17012 (2017)
5. Li host	Li|LFP cell	1.25 mAh cm^{-2}	76% CR after 1000 cycles	1M LiTFSI in DOL/DME (1:1 vol) + 1% $LiNO_3$	**61.5 µL mAh^{-1}**	6.6 µm (1.3 mAh cm^{-2})	J. Am. Chem. Soc. 139, 5916 (2017)
6. Artificial protective layer	Li|NCA cell	3.0 mAh cm^{-2}	96% CR after 400 cycles	1M $LiPF_6$ in EC/DMC (1:1 vol) +10% FEC + 1%VC	**66.7 µL mAh^{-1}**	n/a	Joule 1,394 (2017)
7. Artificial protective layer	Li|NCM 523 cell	1.0 mAh cm^{-2}	90% CR after 400 cycles	1M $LiPF_6$ in EC/EMC (3:7 vol) +10% FEC	**60 µL mAh^{-1}**	400 µm	J. Am. Chem. Soc. 139, 15288 (2017)
8. Li host	Li|LCO cell	0.63 mAh cm^{-2}	85% CR after 140 cycles	1M $LiPF_6$ in EC/DEC (1:1 vol) +10% FEC + 2%VC	**n/a**	300 µm (60 mAh cm^{-2})	Sci. Adv. 3, e1701301 (2017)
9. Electrolyte engineering	Li|NCM 111 cell	2.0 mAh cm^{-2}	80% CR after 700 cycles	1.2 m LiFSI/DMC-BTFE (1:2 mol)	**~100 µL mAh^{-1}**	450 µm	Adv. Mater. 1706102 (2018)
10. Electrolyte engineering	Li|LFP cell	1.0 mAh cm^{-2}	80.8% CR after 1000 cycles	1.0 M $LiPF_6$ and 1.1 wt% LiNO3 in FEC/DMC/DME	**25 µL mAh^{-1}**	500 µm	Angew. Chemie Int. Ed. 57, 5301 (2018)
11. Electrolyte engineering	Li|NCM 111 cell	1.0 mAh cm^{-2}	~80% CR after 250 cycles	1.0 M LiPF6 in EC/DEC electrolyte with sustained-released $LiNO_3$	**80 µL mAh^{-1}**	50 µm	Nature Commun. 9, 3656 (2018)
12. Electrolyte engineering	Li|NCM 111 cell	1.7 mAh cm^{-2}	~80% CR after 500 cycles	2 M LiTFSI + 2M LiDFOB in DME	**41 µL mAh^{-1}**	250 µm	Nat. Energy 3, 739 (2018)
13. Electrolyte engineering	Li|NCM 811 cell	~2.0 mAh cm^{-2}	>90% CR after 120 cycles	1 M $LiPF_6$ FEC/FEMC/HFE	**50 µL mAh^{-1}**	10 µm (2 mAh cm^{-2})	Nature nanotechnology 13, 715 (2018).
This work	Li|NCM 523 cell	1.0 mAh cm^{-2}	77.3% CR after 600 cycles	1M $LiPF_6$ in EC/EMC (3:7 vol) +10% FEC +2% LiBOB	**12 µL mAh^{-1}**	120 µm	
		3.4 mAh cm^{-2}	90.7% CR after 200 cycles	1M $LiPF_6$ in EC/EMC (3:7 vol)+2% LiBOB (no FEC)	**7 µL mAh^{-1}**	33 µm (6.6 mAh cm^{-2})	

Supplementary Table 1 Summary of the state-of-art Li-metal battery performance (updated Jan 2019). This work realized a stable cycling under lean electrolyte conditions.

7. References

1. Fujigaya, T. *et al*. New photoresist materials for 157-nm lithography. Poly[vinylsulfonyl fluoride-co-4-(1,1,1,3,3,3-hexafluoro-2-hydroxypropyl)-styrene] partially protected with tert-butoxycarbonyl. *Chem. Mater.* **15,** 1512–1517 (2003).
2. El Ouatani, L. *et al*. The Effect of Vinylene Carbonate Additive on Surface Film Formation on Both Electrodes in Li-Ion Batteries. *J. Electrochem. Soc.* **156,** A103 (2009).
3. Gao, Y. *et al*. Salt-Based Organic-Inorganic Nanocomposites: Towards A Stable Lithium Metal/Li 10 GeP 2 S 12 Solid Electrolyte Interface. *Angew. Chemie Int. Ed.* **57,** 13608–13612 (2018).
4. Meyer, B. M., Leifer, N., Sakamoto, S., Greenbaum, S. G. & Grey, C. P. High Field Multinuclear NMR Investigation of the SEI Layer in Lithium Rechargeable Batteries. *Electrochem. Solid-State Lett.* **8,** A145 (2005).
5. Gao, Y. *et al*. Interfacial Chemistry Regulation via a Skin-Grafting Strategy Enables High-Performance Lithium-Metal Batteries. *J. Am. Chem. Soc.* **139,** 15288–15291 (2017).
6. Gao, Y. *et al*. General Method of Manipulating Formation, Composition, and Morphology of Solid-Electrolyte Interphases for Stable Li-Alloy Anodes. *J. Am. Chem. Soc.* **139,** 17359–17367 (2017).
7. Li, N.-W., Yin, Y.-X., Yang, C.-P. & Guo, Y.-G. An Artificial Solid Electrolyte Interphase Layer for Stable Lithium Metal Anodes. *Adv. Mater.* **28,** 1853–1858 (2016).
8. Li, G. *et al*. Organosulfide-plasticized solid-electrolyte interphase layer enables stable lithium metal anodes for long-cycle lithium-sulfur batteries. *Nat. Commun.* **8,** 850 (2017).
9. Foroozan, T. *et al*. Synergistic Effect of Graphene Oxide for Impeding the Dendritic Plating of Li. *Adv. Funct. Mater.* **28,** 1705917 (2018).